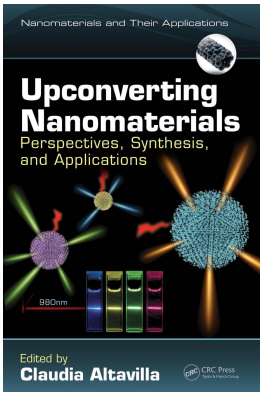

Upconverting Nanomaterials Perspectives, Synthesis, and Applications

Claudia Altavilla

Synergistic Effects in Organic-Coated Upconversion Nanoparticles

Publication details
https://test.routledgehandbooks.com/doi/10.1201/9781315371535-7
Laura Francés-Soriano, María González-Béjar, Julia Pérez-Prieto
Published online on: 10 Oct 2016

5

Synergistic Effects in Organic-Coated Upconversion Nanoparticles

Laura Francés-Soriano, María González-Béjar, and Julia Pérez-Prieto

CONTENTS

5.1 Introduction

Lanthanide-doped upconversion nanoparticles (UCNPs), such as $NaYF_4$ doped with Yb^{3+} and Er^{3+}, exhibit narrow and high-intensive emissions in the visible spectrum when excited by a low power energy, continuous-wave (CW) near-infrared (NIR) laser, that is, a large anti-Stokes shift (see Figure 5.1). Of special relevance for biomedical applications, NIR light exhibits a remarkably deep penetration into tissues, and UCNPs present luminescence with a high signal-to-noise ratio, they are very resistant to photobleaching and photoblinking, they exhibit excellent chemical and thermal stability and relatively low toxicity, and they are suitable for long-time particle tracking (G. Chen et al. 2014; Dacosta et al. 2014; Gnach et al. 2015; Gu et al. 2013; Y. Liu et al. 2013; M. Wang et al. 2011). These unique properties not only make UCNPs particularly ideal in nanomedicine, but they are also promising in nanotechnology, since they can be used for photovoltaic cells (as NIR absorbers), photocatalysis (as sensitizers), and security applications (anti-counterfeiting materials) (G. Chen et al. 2015; Gnach and Bednarkiewicz 2012; Ramasamy et al. 2014; Won Jin et al. 2009).

A general feature common to all nanoparticles (NPs) is that they possess a high surface-to-volume ratio. By making use of this property, NPs can be capped with a considerable number of ligands, which have an anchoring atom at one end with affinity for the NP surface and the other end provides the NP periphery with the hydrophobicity or hydrophilicity needed to give rise to stable organic or aqueous NP colloidal solutions, respectively (See Figure 5.2) (Sedlmeier and Gorris 2015).

A highly relevant role that ligands can also play is that of introducing additional functionality to the nanosystem. In this case, the NP acts as a 3D-scaffold which makes it possible to provide a high local concentration of a functional moiety, such as fluorophores and photosensitizers. The UCNP combined with its organic capping can act as a nanohybrid with properties that differ from those of the individual components (Wolfbeis 2015). This symbiotic effect arises not only from the possibility of placing a high local concentration of a functional group on the NP surface, but

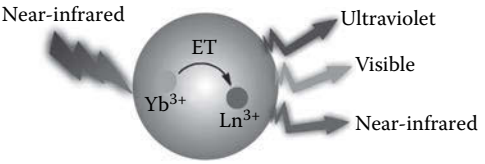

FIGURE 5.1
UCNP emission after excitation with NIR light.

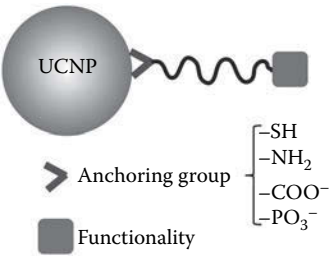

FIGURE 5.2
General representation of organic ligand coated UCNPs.

also from the potential incorporation of simultaneous functionalities on the NP capping, the high encapsulating capacity of the nanohybrid, the capacity of the ligand to produce an efficient interdigitation of amphiphilic molecules and the potential of the ligand to be used for establishing specific interactions, among others (Sedlmeier and Gorris 2015; Wolfbeis 2015). The symbiosis between NPs and their ligands enhances the unique properties of the upconversion (UC) material and the nanohybrid can be applied in molecular recognition, drug-delivery, phototherapy, and so on. Figure 5.3 shows a scheme of possible modifications which will be discussed in the following section.

In this chapter, strategies recently devised for the preparation of smart photoactive UCNPs will be analyzed in terms of the symbiotic effect between the organic and the inorganic components.

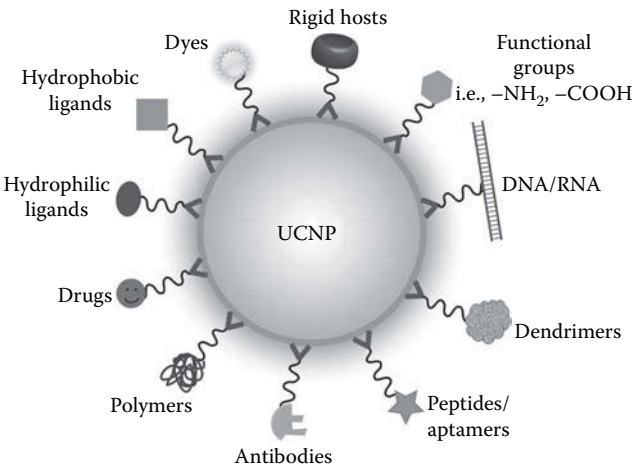

FIGURE 5.3
Possible modifications of UCNPs with organic ligands.

5.2 A Brief Explanation of Upconverting Nanomaterials

5.2.1 The Upconversion Phenomenon

NIR light can be used to excite UCNPs in complex mixtures that contain chromophores which absorb ultraviolet–visible (UV–Vis) light powerfully and this makes them relevant for biological and nanotechnological applications (Idris et al. 2015).

The UC process in lanthanides involves the sequential absorption of two or more NIR photons and it can take place via three competitive mechanisms: excited state absorption (ESA), energy transfer upconversion (ETU), and photon avalanche (PA), Figure 5.4a (Auzel 2004; Tu et al. 2015). These mechanisms differ in how the multiphoton absorption process occurs. In the ESA process, there is a successive absorption of two photons by a single ion: (1) the first photon is resonant with the transition from the ground state (GS) level to the excited metastable (ES1) level and (2) the second photon possesses energy that is resonant with the transition from ES1 to the higher excited state ES2. Then, the photon drops from ES2 to GS and the UC emission

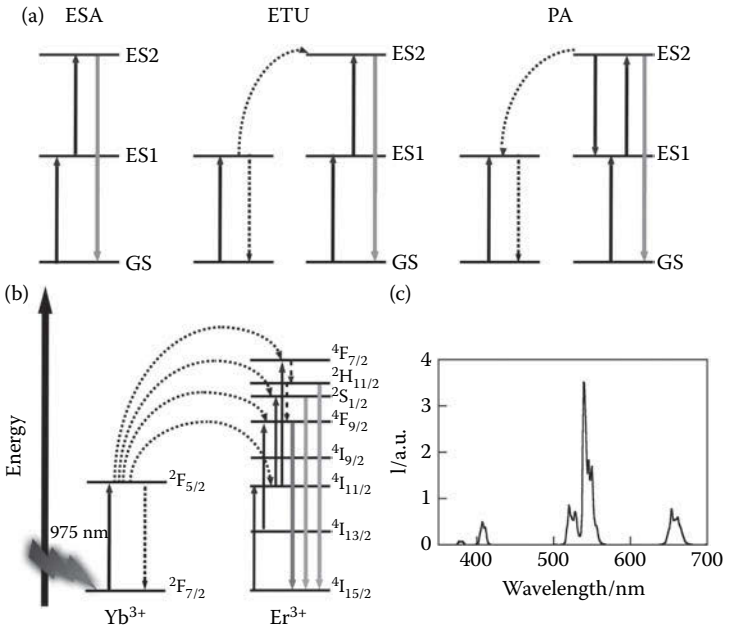

FIGURE 5.4
(a) UC processes for lanthanide-doped crystals: ESA, ETU, and PA. (b) Schematic representation of the ETU mechanism for a host matrix doped with Yb and Er ions; the dashed/dotted, dashed, and full arrows represent photon excitation, energy transfer, and emission processes, respectively, and (c) Emission spectrum (λ_{ex} = 975 nm) of $NaYF_4$:Yb, Er UCNPs.

occurs. This mechanism requires the concentration of the active ion to be low to avoid transfer loss through cross-relaxation between the luminescent centers and it is suitable for single-doped materials.

The ETU mechanism is based on a sequential absorption of two photons to populate the ES2 level. The main difference between ETU and ESA is that the excitation in ETU occurs through energy transfer between two adjacent ions. In the ETU process, each of two adjacent ions can absorb a photon of the same energy, thereby populating their excited level. A nonradiative energy transfer process promotes one of the ions to the upper ES2 and eventually leads to ES2–GS emission, while the other ion relaxes back to GS (Auzel 2004). In this type of UC process, the concentration of ions, which determines their average distance, has a strong influence on the UCNP emission efficiency. This is the most frequently observed and developed mechanism in UCNPs (Naccache et al. 2015).

In the PA process, the ES1 level of an ion is reached by a nonresonant excitation and then a cross-relaxation energy transfer occurs between the excited ion and the adjacent ion at the GS, thus resulting in the population of the intermediate level ES1 of both ions after a number of excitation cycles; the ES1 level acts as a storage reservoir for pumping energy. Subsequently, the two ions readily populate the ES2 level to initiate further cross-relaxation and the ES2 population increases exponentially, finally resulting in a strong UC emission as an avalanche process. The PA mechanism requires the pump intensity to reach a threshold value to generate a robust photocycle (Auzel 2004). This process suffers from several drawbacks, such as a strong dependence on the pump power and a slow response to excitation (up to several seconds) due to numerous looping cycles of cross-relaxation processes. This mechanism is hardly ever observed.

Figure 5.4b depicts the ETU mechanism for an UCNP consisting of a host matrix doped with Yb and Er ions. For this system, an electron of the Yb^{3+} is excited from the $^2F_{7/2}$ to $^2F_{5/2}$ level, and then the Yb^{3+} excited state transfers its energy to the Er^{3+} leading to the $^4I_{11/2}$ excited state. During the population of $^4I_{11/2}$, a second Yb^{3+}excited state transfers its energy to this level, thus populating a higher $^4F_{7/2}$ excited state of the Er^{3+} ion. The Er^{3+} ion can then relax nonradiatively to the $^2H_{11/2}$ and $^4S_{3/2}$ levels, leading to green emissions at 525 and 543 nm (Figure 5.4b). Competitively, the electron can further relax and populate the $^4F_{9/2}$ level, thus leading to a red emission at 659 nm. These are two-photon processes, but three-photon processes can also be observed, mainly when using a high pumping power. In the case of the Yb/Tm pair, two-, three-, and four-photon processes can be observed with emissions at 695 and 800 nm (two-photon), 450 and 650 nm (three-photon), and 360 and 450 nm (four-photon).

Whereas two-photon absorption processes are observed in some organic chromophores and NPs, such as CdSe quantum dots, that occur via "virtual states," the ETU in UCNPs occurs via the real long-lived excited states of the rare-earth ions in the UCNPs. As a consequence, UC luminescence can be

observed by using inexpensive CW diode lasers with a moderate excitation power density of ca. 10 W cm^{-2}. By contrast, the simultaneous two-photon absorption processes in dyes require expensive ultra-short-pulsed lasers with high power density excitation (10^5–10^9 W cm^{-2}).

5.2.2 Upconversion Materials

The UC material is composed of a host matrix doped with an activator and a sensitizer, which are both rare earth (RE) ions (Gai et al. 2014). Whereas the sensitizer only possesses one excited state, the activator has ladder-like energy levels and the energy difference between three or more subsequent levels is close to that of the energy separation between the GS of the sensitizer and its single excited state in order to make the multiple photon absorption and energy transfer possible. The sensitizer possesses a higher absorption cross-section at the NIR region than the activator (e.g., 10 $M^{-1}cm^{-1}$ for Yb^{3+} vs. about 1 $M^{-1}cm^{-1}$ for Er^{3+}). The concentration of the sensitizer in the host matrix is larger than that of the activator to enhance the energy transfer from the sensitizer to the activator and to avoid self-quenching effects of the activator. Er^{3+}, Tm^{3+}, and Ho^{3+} are generally selected as activators for UC photoluminescence (Gai et al. 2014; Schäfer et al. 2007).

The host matrix plays a crucial role in the UC process. It should be taken into account that the $4f^n$ transitions of the RE ions (emissive species) are strongly forbidden by the parity selection rule (Naccache et al. 2015). As a consequence, the lanthanide ions usually exhibit low molar absorption coefficients and their excited states are long-lived (from μs to ms).

These transitions are perturbed by static crystalline fields and therefore they become partially allowed in the host matrix. This host lattice effect explains the higher emission of the bulk UC material than that of the nanoparticle, as well as the decrease of the emissive efficiency of a nanoparticle as its size decreases, specifically, the ratio of RE ions near the NP surface increases and the perturbation by the crystalline field decreases. The ions at the NP surface behave as "dormant ions."

In addition, the ideal host materials should offer a dense lattice to the dopant and should possess low lattice phonon energy. As the RE^{3+} ions and alkaline ions exhibit similar ionic sizes, their inorganic compounds are a good choice to reduce lattice impurities, which would quench the UCNP luminescence (Schäfer et al. 2007). A matrix with low phonon energy minimizes the highly competitive nonradiative processes, thus resulting in more emissive UCNPs. The most popular inorganic host materials for UCNPs are RE fluorides, since they have low phonon energies (about 350 cm^{-1}) and high chemical stability (Haase and Schäfer 2011).

In addition, the crystal structure phase of the host material is highly relevant for the emissive properties of the UCNP. Thus, the thermodynamically stable hexagonal (β) phase $NaYF_4$ (β-$NaYF_4$) is more suitable than the cubic (α) phase (α-$NaYF_4$), since the former is of lower symmetry. As a result,

the intensity of the green emission of β-$NaYF_4$: Yb, Er is 10 times higher than that of the cubic phase.

There are several strategies to increase the luminescence efficiency of UCNPs. For instance, the dormant ions near the UCNP surface can become active ions by formation of an undoped shell of the same material as the host matrix (e.g., $NaYF_4$:Yb, Er@$NaYF_4$). This strategy has resulted in up to 30-fold enhanced emission compared to that of the core; this is ascribed to the shell crystalline field effect. In addition, the growth of a silica shell also results in more emissive UCNPs (e.g., $NaYF_4$:Yb, Er@SiO_2) (Xie et al. 2013). The enhanced emission due to the noncrystalline shell can be attributed to its low phonon energy and/or to an increased perturbation due to the ligand field effect. The improved spontaneous emission rate is also consistent with an enhanced local density of states brought about by the change of the refractive index at the interface between the core and the shell.

Moreover, it has also been demonstrated that the use of a fluoride host matrix with ytterbium instead of yttrium is beneficial for the UCNP efficiency. Thus, the NIR-to-NIR photoluminescence of $NaYbF_4$:Tm (2%) was four times higher than that of $NaYF_4$:Yb (20%), Tm (2%) (Chen et al. 2010).

In summary, UCNPs can be capped with an inorganic shell, whose role is to increase their luminescence (by reducing the amount of surface defects and/or isolating them from interactions with emission quenchers).

Furthermore, the organic capping can also be beneficial for the emissive properties of the UCNP although high energy C–H and C–C vibrational oscillators reduce the emission through nonradiative relaxation processes (this quenching effect is more important for long chains) (Heer et al. 2004; Suyver et al. 2005).

Although there are several strategies to enhance the emission of UCNPs, the quantum yield (Φ_f) of an UC process, defined as the ratio of photons absorbed by a fluorophore to those emitted via fluorescence, is quite low; two or more photons are required for UC emission and, therefore, its efficiency depends not only on the absorption cross-section of the sensitizer at the excitation wavelength but also on the power density of the excitation source, and as mentioned above it also depends on the particle size. Thus, the Φ_f of the green emission of $NaYF_4$:Er,Yb UCNPs at 150 W cm^{-2} power density changes from 0.005% to 0.1% to 0.3% when the nanoparticle size changes from 8–10 nm to 30 nm to 100 nm (Boyer and Van Veggel 2010). In addition, at a considerably lower power density (20 W cm^{-2}), the Φ_f of bulk $NaYF_4$:Er,Yb is 3.0%.

5.2.3 UC Material Multicolor Emission and Its Tuning

The relative intensities of the different emission peaks of UCNPs can be changed accurately by varying the dopant ion concentration, mainly that of the sensitizer (Li and Lin 2010). Thus, the green-to-red emission of $NaYF_4$:Yb, Er decreases by increasing Yb^{3+} concentrations. This has been ascribed to

the decrease of the Yb–Er interatomic distance, which facilitates the back energy transfer from Er^{3+} to Yb^{3+}. Thus, the output color of these NPs has been changed from green to yellow (combination of red and green) and then to red by increasing the concentrations of Yb^{3+} ion (Guo et al. 2012).

The output emission of the UCNP also depends on the nature of the dopant ions. Thus, $NaYF_4$:Yb, Tm UCNPs emit blue since they possess a dominant emission in the visible at ca. 470 nm together with a weak one at ca. 650 nm, as well as a stronger emission in the NIR (at 800 nm).

In addition, the UCNP emission output can also be manipulated by using inorganic perovskites as host matrices (such as $KMnF_3$:Yb, Er), thus leading to UCNPs with a high-purity single-band emission (red emission in this case) (Lei et al. 2015). This is ascribed to an efficient nonradiative energy transfer from the level responsible for the green emission ($^2H_{11/2}$ and $^4S_{3/2}$ of Er) to the ^1T level of Mn^{2+}, followed by back energy transfer to the level responsible for the red emission ($^4F_{9/2}$ level of Er).

Finally, a white emission can be obtained by using a three-component dopant system. For example the $NaYF_4$:Yb,Er, Tm combines the red and green emissions of Er with the blue of Tm. The output emission of the system can be varied from blue to white by gradually increasing the Er concentration, that is, by increasing the intensity of the green and red emissions.

5.2.4 The Ligand Anchoring Group

Though the UCNPs can also be prepared as "naked" systems (Bogdan et al. 2011; A. Dong et al. 2011), they are usually covered with an organic capping (UCNP@organic capping), whose role is to keep them isolated and make them dispersible (in either organic and/or aqueous media) or even to provide them with an additional functionality. The organic ligand can play a key role in different stages of a nanoparticle, such as in its preparation, dispersibility in a medium, optical performance, and application in different areas.

Obviously, core and core–shell UCNPs (shell refers to inorganic materials) will eventually be capped by an organic capping, either by surface modification, for example, silica, or by noncovalent binding (Muhr et al. 2014).

Therefore, several strategies can be combined to obtain the best synergy possible between the organic coating and the UCNPs. In fact, the role of the organic capping is not only to determine the dispersibility of a nanoparticle in a specific medium, but also to provide the nanosystem with additional functionality and/or impede the UCNPs from causing any undesirable interference with the environment (e.g., cellular) or their aggregation. Therefore, the organic capping should remain firmly anchored to the UCNP.

Organic ligands are attached to the UCNP surface via an anchoring group (Figure 5.2). The most typical groups are NH_2 (e.g., oleylamine (OM)), SH (e.g., polyethyleneglycol [PEG]-SH (Voliani et al. 2013)), COOH (e.g., oleic acid (OA)), and PO_3H (e.g., PEG-PO_3H (Boyer et al. 2010)). However, gradual desorption of the ligands from the NP surface occurs due to the noncovalent

linkage. This desorption can be decreased by using multichelating ligands, such as polymers and dendrimers. Among multichelating polymers are (i) polyacrylic acid (PAA) and polyanionic dendrimers with carboxylate groups, (ii) poly (amidoamine) and branched polyethylenimine (PEI) with amino groups, (iii) p(MEO_2MA-co-SEMA) copolymer (where MEO_2MA is 2-(2-methoxyethoxy)ethyl methacrylate and SEMA is thiolate-containing methacrylate) with thiolate groups, polyphosphoric acid with phosphonic groups, and (iv) polyvinylpyrrolidone (PVP) with amide groups (Cheng and Lin 2015; Liras et al. 2014).

In addition, rigid dendrimers have been used as the organic capping of UCNPs. These dendrimers are anchored to the UCNP surface via carboxylate groups, but their globular shape permits a large number of the carboxylates to be at the nanoparticle periphery, thus enhancing the water-dispersibility of the UCNPs as well as offering the possibility of further conjugation (Esipova et al. 2012). The most typical anchoring group of UCNPs is the carboxylate. However, the carboxylic acid pKa is ca. 5 (e.g., in OA) and therefore the carboxylate anchoring group becomes progressively protonated in acidic media and consequently the carboxylic ligand eventually separates from the UCNP surface. In fact, this is the strategy (protonation of oleate-capped UCNP (UCNP@OA) at pH below 4) used to prepare "naked" UCNPs (Bogdan et al. 2011). Leaching does not only apply to carboxylate ligands but also to ligands anchored via other groups.

5.3 Synergistic Effects between the UC Nanomaterial and the Organic Ligand

The *organic ligand* can be crucial at different stages of a nanoparticle, from the nanoparticle preparation to its dispersibility in a medium, from its optical performance to its application in different areas. *The nanoparticle* can act as a carrier of functional organic molecules, making it possible to increase the local concentration of a functional molecule. In addition, *the nanoparticle and its organic ligand* can cooperate to encapsulate functional molecules close to the nanoparticle surface. Examples of the synergistic effect between the inorganic component (the nanoparticle) and the organic component (the organic ligand) as well as its relevance to provide smart nanosystems will be presented in the following sections.

5.3.1 The Role of the Ligand in the Preparation of the Nanomaterial

Upconverting nanomaterials can be prepared by several methods: coprecipitation, thermal decomposition, hydro(solvo)thermal synthesis, sol–gel processing, and combustion synthesis (Chen et al. 2012; Wang and Liu 2009).

The reaction temperature, time, and composition of the reaction mixture can determine the size, phase, or morphology of the UCNPs (Chen et al. 2012; Guo et al. 2012; Naccache et al. 2015; Pan et al. 2013; Voliani et al. 2014; Wei, et al. 2006; Yang et al. 2012; Ye et al. 2010).

However, the anchoring ligand can also play a crucial role on such features. These NPs are usually synthesized in the presence of a noncoordinating solvent with a high boiling point (octadecene, ODE) and a capping ligand (OA) that prevents their agglomeration (Chan 2015; Li and Lin 2010; M. Wang et al. 2011) and makes them dispersible in organic solvents (F. Zhang). Alternatively, other solvents/ligands, for example, trioctylphosphine (TOP) (Shan and Ju 2009), OM (Yi and Chow 2006), and trioctylphosphine oxide (TOPO) (Zhuravleva et al. 2005) can be used for the synthesis of UCNPs.

The amount of ligand employed during the synthesis can determine the shape of the resulting UCNPs (Guo et al. 2012; Li and Zhang 2008; Mai et al. 2006; Zhang et al. 2005). Li and Zhang showed that the ligand concentration in the reaction mixture affects the growth rate of the nanocrystals in the [100] and [001] directions. It is faster in the [100] direction at low ligand concentration, both rates are similar when the ligand concentration increases, and it is faster in the [001] direction at high concentrations. Therefore, hexagonal nanoplates, spherical nanocrystals, and elliptic nanocrystals can be obtained by changing the ligand concentration. Similar results have been obtained by J. Guo et al. when increasing the concentration of OA.

H.-X. Mai et al. have found that addition of small amounts of OM to the reaction mixture containing OA/ODE increases the energy barrier between α-$NaReF_4$ and β-$NaReF_4$ phases and consequently, the presence of large amounts of OM decreases the growth rate of β-$NaReF_4$.

In addition, OA/OM/ODE mixtures can lead to ultrasmall UCNPs (7–10 nm) which are attractive for bioimaging, since they are easily eliminated from the body (Chen et al. 2010). Alternatively, ultrasmall hexagonal $NaYF_4$:Yb,Er(Tm) UCNPs can be obtained by using OM as both ligand and solvent (Yi and Chow 2006). The coordination of lanthanide cations with amines is weaker than with carboxylate groups and OM facilitates the phase transition of $NaYF_4$:Yb,Er(Tm) from cubic to hexagonal in comparison with OA.

Also, TOP has been used as capping ligand in combination with OA (Shan and Ju 2009; Shan et al. 2007) to lead to OA–TOP co-capped $NaYF_4$ NPs. TOP is crucial in stopping the NPs from aggregating and allowing the three-dimensional growth of NPs to obtain hexagonal nanoprisms. The cooperative action between TOP and OA decreases the energy barrier of the α-to-β-phase transition, thus allowing the synthesis of β-UCNPs at lower temperatures (Shan and Ju 2007).

Yang et al. (2012) have demonstrated the involvement of the organic capping ligand in the final shape of the particles prepared by hydrothermal synthesis by using bifunctional carboxylic compounds, namely malonic acid (MA), oxalic acid (OXA), succinic acid (SA), and tartaric acid (TA). One of

the carboxylic group anchors to the particle surface, whereas the other can be used for further functionalization of the particle periphery. The shape of the material changes from rods to hexagonal prisms, hollow prisms, and tubes by increasing the amount of MA. Differences in acidity result in differences in the anchoring capacity of the carboxylic acids to the crystal surface and in the growth direction. Thus, disks, polygonal columns, and hexagonal tablets are obtained by using OXA, SA, and TA, respectively.

Therefore, though an exhaustive study about the influence of the ligand in the preparation of UCNPs is still lacking, the above-mentioned data are consistent with the role of the ligand anchoring group in the phase, size, and morphology of the resulting UCNP.

5.3.2 The Role of the Ligand in the Colloidal Stability of UCNPs in Aqueous and Nonaqueous Solvents, as Well in the UCNP Phase Transfer

The ligand on the UCNP surface avoids their aggregation thanks to steric or electrostatic repulsions and makes the UCNPs dispersible in organic or aqueous media (Sedlmeier and Gorris 2015). Apolar ligands provide lipophilicity to the nanoparticle surface, whereas polar ligands, which after anchoring to the UCNP surface provide polarity to the UCNPs surface, make the UCNPs hydrophilic.

In general, the UCNPs are synthesized in the presence of hydrophobic ligands (OA, TOP, and OM), but they can be become water-dispersible or amphiphilic through surface modification by ligand exchange, ligand oxidation, electrostatic interactions, layer by layer assembly, bio-conjugation, polymerization, silanization…(Muhr et al. 2014; M. Wang et al. 2011).

Moreover, these modifications can be beneficial for the optical properties and/or functionality (see Figure 5.3) of the NPs but these points will be discussed in Sections 5.3.3; 5.3.4; and 5.3.5. One of the most common strategies to obtain the UCNP with the desired functionality is ligand exchange, that is, the displacement of the original ligand by another ligand which can provide new properties or functionalities. The new organic ligand has to bind more strongly to the surface of the nanoparticle to allow a fast and effective displacement. Some examples are discussed below.

Poly(allylamine) (PAAm) replaces the ligand of oleate-capped $NaYF_4$:Yb, Er NPs at room temperature, thus leading to hydrophilic NPs. However, it requires prolonged reactions times (about 36 h) due to the strong interaction between the carboxylate group of the oleate and the UCNP surface (Xia et al. 2014). An increase of the reaction temperature can shortcut the reaction time as it has been shown in the exchange using PEG-SH to produce water-dispersible, PEG-capped UCNPs (heating at 60°C overnight) (Voliani et al. 2013). The use of a tetraprotonic acid, namely 1-hydroxyethane-1,1-diphosphonic acid (HEDP), shortens further the reaction time and hydrophilic UCNPs can be successfully prepared after stirring the reaction mixture at

60°C during 4 h (Schäfer et al. 2007). Therefore, the direct ligand exchange strategy needs the optimization of parameters such as concentration, stirring time, and temperature for each ligand. Moreover, NPs can aggregate during the ligand exchange (B. Dong et al. 2011). Hence, the direct ligand exchange can be a relatively difficult strategy with a tedious work-up and be time-consuming (from 4 h to several days) (Muhr et al. 2014).

Ligand exchange reactions involving two steps can be advantageous: first, the OA ligand is removed via acid treatment or by reacting with $NOBF_4$ and then new ligands, such as OM, PVP, cucurbit[n]uril (CB), and polyglutamic dendrimers, are easily attached to the NPs (Esipova et al. 2012; Francés-Soriano et al. 2015; Muhr et al. 2014). This method reduces significantly the aggregation of the UCNPs during the ligand exchange and allows for the attachment to the nanoparticle surface of any organic capping agent with an appropriate anchoring group (Muhr et al. 2014).

While ligand exchange involves a replacement of the original ligand by a new ligand, the colloidal stability of UCNPs in water can be improved by adding a new layer of organic coating via ligand attraction with the original ligand. There are three possibilities: (i) hydrophobic interactions with amphiphilic polymers or surfactants, (ii) electrostatic interactions, or (iii) host–guest interactions.

The use of amphiphilic polymers or surfactants is the most common strategy. The long alkyl chains of the polymers or surfactants intercalate between the chains of OA-capped UCNPs via van der Waals interactions, while the hydrophilic groups or chains of the polymer are in the nanosystem periphery and therefore the NPs are dispersible in water (Muhr et al. 2014).

Amphiphilic polymers, such as PEI (Yan et al. 2013), PEG (C. Wang et al. 2011), PAA (Yi and Chow 2007), N-succinyl-N′-octyl chitosan (SOC) (Cui et al. 2012) can transfer UCNPs from nonpolar solvents to water via hydrophobic interactions while maintaining the original ligand. PEI-modified graphene oxide (PEI-GO) was used as nanocarrier of UCNPs to prepare water-dispersible NPs (Yan et al. 2013). A water solution of PEI-GO was added to a chloroform dispersion of UCNP@OA forming a biphasic system. Authors observed that, after stirring this system, UCNPs were transferred to aqueous phase due to the hydrophobic interaction between the hydrophobic plane of PEI-GO and oleate alkyl chains on the surface of UCNPs, whereas the hydrophilic plane made the dispersibility of UCNPs possible in aqueous media and physiological solutions.

In addition, it has been shown that the hydrophobic chains of the PEG-grafted poly(maleic anhydride-alt-1-octadecene) can interact via van der Waals with the lipophilic chain of oleate on the UCNP surface, whereas the hydrophobic outer groups allow the dispersibility of UCNPs in water (See Figure 5.5) (C. Wang et al. 2011). Analogous interactions were observed between alkyl chains of OM-capped $NaYF_4$:Yb, Tm, and isopropyl groups in the modified PAA polymer, thus resulting in hydrophilic NPs due to

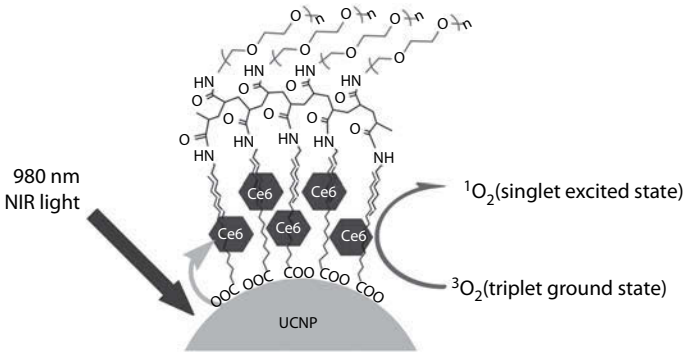

FIGURE 5.5
Schematic drawing showing NIR-induced singlet oxygen generation using of Ce6 encapsulated in PEGylated UCNPs (J. Liu et al. 2013). (Reprinted from *Biomaterials*, 32/26, Wang, C., H. Tao, L. Cheng, Z. Liu, Near-infrared light induced *in vivo* PDT of cancer based on UCNPs, 6145–6154, Copyright 2011, with permission from Elsevier.)

carboxyl groups of the modified PAA extending outward (Yi and Chow 2007).

Furthermore, surfactants, such as TWEEN 80 or cetyltrimethylammonium bromide (CTAB) can be used to convert hydrophobic UCNPs NPs into hydrophilic ones (Ren et al. 2012). The TWEEN surfactant is very cheap and it can prevent the nonspecific adsorption of proteins. Hydrophobic interactions between the lipophilic tails of TWEEN and the oleate layer on the surface of UCNPs allow ligand interdigitation and the UCNPs are transferable from an apolar solvent to water, biological buffers, and culture media.

Also, cationic CTAB, an ionic sodium dodecyl sulfate and nonanionic PEG tert-octylphenyl ether (C_8PhE_{10}) surfactants were successfully interdigitated to the nanoparticle ligand (Liang et al. 2012). High concentrations of surfactant gave rise to bilayer-modified individual UCNPs while at lower concentrations the aggregation of the UCNPs was observed. Interestingly, the bilayer-modified UCNPs can facilitate the nanoparticle silication, thus improving the stability of the nanosystem and enhancing their application.

In addition, hydrophobic UCNPs can be transferred to aqueous media via electrostatic interactions between organic capping layers. For example, multilayer nanohybrids can be built via electrostatic attractions between different layers of positively charged poly-(allylamine hydrochloride) (PAH) and negatively charged poly(sodium 4-styrenesulfonate) (PSS). Thus, UCNPs were negatively charged and could interact via electrostatic attraction with positively charged PAH, forming a layer of PAH around the NPs. After that, a negatively charged layer of PSS was added and subsequently assembled with PAH again. This method is known as layer-by-layer surface modification and makes it easy to control the shell thickness (Wang et al. 2005).

Another efficient and simple strategy to transfer hydrophobic NPs into water is by using host–guest interactions, such as that between β-cyclodextrin (CD) and adamantaneacetic acid (ADAA) (Liu et al. 2010). Thus, UCNP@ADAA NPs were transferred to a water solution containing CD by forming the UCNP@ADAA@CD nanohybrid.

5.3.3 The Role of the Ligand in the Optical Properties of the Nanomaterial

The emission ion of UCNPs is usually quenched to a higher extent in the presence of water molecules or alcohols than in organic solvents (Arppe et al. 2015; Wilhelm et al. 2015). Therefore, the way in which the modification of the UCNP is carried out to make them water dispersible is crucial for their final emission efficiency (Wilhelm et al. 2015).

A useful strategy to obtain nanohybrids dispersible in water while keeping or enhancing their emission is to use multi-anchoring polymers that meet two requirements: they must be firmly attached to the UCNP surface, thus avoiding the direct contact with water molecules, and they must provide hydrophilicity to final UCNP@polymer nanohybrids.

For instance, β-$NaYF_4$:Yb,Er, UCNPs have been capped with a thin polymer shell by replacing the oleate ligand of UCNPs by multidentate thiolate-grafting of P(MEO_2MA-*co*-SEMA) copolymers (Liras et al. 2014). The presence of the 2-(2-methoxyethoxy)ethyl side chains of MEO_2MA extending out of the nanohybrid made them water-dispersible, whereas the part anchoring to the surface was hydrophobic and prevented water from approaching the UCNP surface as opposed to ligands with a polar chain, such as PEG (Voliani et al. 2013). Interestingly, the amphiphilic nature of the UCNP@P(MEO_2MA-*co*-SEMA) nanohybrids made it possible to compare the emission in dichloromethane of the UCNP@polymer nanohybrids with that of UCNP@OA, thus showing that the nanohybrids exhibit enhanced emission by a factor of up to 10 compared with that of UCNP@OA. Moreover, the emission of the UCNP@polymer nanohybrids in water is even twofold greater than that of UCNP@OA in chloroform. The emission enhancement provided by the polymer can be explained by the reduction of surface defects and/or the isolation the UCNP from interactions with emission quenchers.

In addition, it has recently been reported that both the emission performance and the intensity ratio of the red and green UC emission bands of water-dispersible β-$NaYF_4$:Yb, Er UCNPs depend on the surface modification strategy chosen for their preparation from hydrophobic UCNPs (in particular, UCNP@OA) (Wilhelm et al. 2015). The deposition of an amphiphilic polymer on the top of the UCNP@OA exhibited reduced nonradiative quenching by water as compared to UCNPs prepared via ligand exchange. Moreover, the bilayer UCNPs showed a brighter green luminescence compared to the intensity of the red emission, whereas ligand exchange led to the opposite.

This trend was hardly affected by the chemical nature of the ligand (Wilhelm et al. 2015).

5.3.4 The Role of the NPs in the Organic Ligand Functionality

As mentioned above, the organic ligand can modulate important features of the UCNP, such as dispersibility, emission efficiency, as shown in UCNP@P(MEO_2MA-*co*-SEMA) nanohybrids, where the polymer provides the nanoparticle with amphiphilic and thermosensitive properties due to the lateral ethylene glycol chains. Consequently, they exhibit reversible aggregation/disaggregation above and below the lower critical solution temperature, respectively (Liras et al. 2014).

Interestingly, the nanoparticle can modulate the properties of the organic capping. Thus, the lower critical solution temperature value changed drastically for these polymers covalently bound to the nanoparticle surface and it was about that of human body temperature in some of them. This can be ascribed to the flexibility of the polymers to adopt suitable conformations to anchor the UCNP surface.

5.3.5 Synergism in the Nanohybrid Functionality

5.3.5.1 Functionality

It is important to highlight that the large surface/volume ratio of the NPs makes it possible to decorate them with a high number of functional groups at the periphery by choosing the proper organic capping. For example, UCNPs coated with PEGs with an anchoring group in one end and amino and/or carboxylic groups at the other can be further conjugated with other functional molecules by performing simple coupling reactions (either coupling of amine-functionalized molecules to the free carboxylates on the nanohybrid periphery or coupling of carboxylic-functionalized groups to the amine groups on the nanohybrid periphery). This strategy has been applied to the preparation of water-dispersible UCNPs with two different payloads (fluorescein and rhodamine derivatives) by using two orthogonally functionalized PEGs (Voliani et al. 2013). More examples of the symbiosis of the UCNP and the organic capping to provide additional functionality will be discussed in the following sections, since they have been designed for specific applications.

5.3.5.2 Synergistic Effect between the UCNP and the Organic Ligand in the Nanosystem Functionality: Encapsulation versus Ionic and Covalent Binding

The nanoparticle and the organic capping can work together to endow the nanohybrid new capacities as compared to that of the individual components, that is, the naked nanoparticle and the ligand. In principle, the ligand

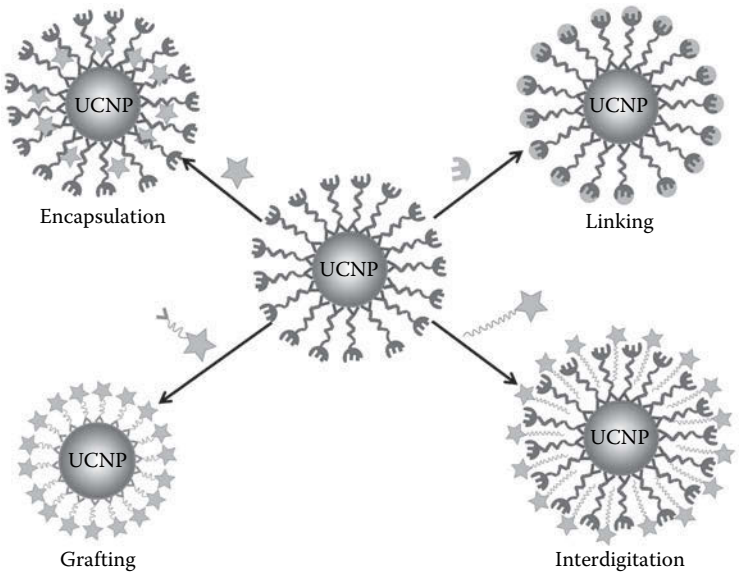

FIGURE 5.6
Schematic representation of the mechanisms to add functionality to the UCNP.

can be a molecule whose primary target can be to decorate the nanoparticle periphery in such a way that permits the further binding of functional molecules, such as, biomolecule, photosensitizer (PS), and drug.

Figure 5.6 illustrates different strategies to add functionality to the UCNPs via the organic capping: (i) covalent or ionic linkage of functional organic molecules to the ligand functional group; (ii) interdigitation between the chains of the organic ligand and functional molecule, either surfactant or polymer; and (iii) encapsulation of the functional molecule within the nanoparticle organic capping. This chapter is devoted to the synergistic effects between UCNPs and the organic ligands; UCNP refers to both NPs with and without an inorganic shell. Thus, core UCNPs capped with inorganic shells, such as silica and titanium dioxide, will be mentioned throughout the chapter, but the emphasis will be placed in the role of the organic capping.

Most of the examples reported in the literature benefit from the covalent bonding between groups, such as carboxylic, amines, and thiols, to locate functional (bio)molecules at the periphery of organic-capped UCNPs. However, there are also examples of noncovalent bonding, such as dipole-ionic and van der Waals interactions.

With regard to ionic binding, UCNPs capped with cucurbiturils (UCNP@CB hybrids) have been used as scaffolds for cationic dyes (such as methylene blue and pyronin Y), due to their anchoring to the CB free carbonyl portal (a charge–dipole interaction) (Francés-Soriano et al. 2015). This made it possible to locate a high concentration of the dyes close to the UCNP and lead to

efficient energy transfer from the UCNP to the dye. These UCNP@CB@dye supramolecular systems may be highly advantageous in photodynamic therapy (PDT) taking into account the interest of these tricyclic basic dyes in PDT.

It is also possible to use bi-layer water-dispersible nanohybrids to encapsulate nonpolar organic molecules, for example, to load chlorin e6 (Ce6) within the hydrophobic part of the organic capping (see Figure 5.5) (J. Liu et al. 2013).

5.3.5.3 Targeting

Target ability refers to the selective delivery of UCNPs to diseased tissues and is of high relevance for biomedical applications. A specific interaction between the surface ligand and cells or biomolecules is needed in order to minimize damage to normal tissues. Small molecules, peptides, proteins, aptamers, dendrimers, carbohydrates, and antibodies anchored on the UCNP surface or linked to the UCNP ligand can be recognized by specific cells (Friedman et al. 2013). Targeting can be combined with other applications of UCNPs, such as drug delivery, sensing, and bioimaging. These applications will be discussed in the following sections.

Small molecules such as carbohydrates (Bogdan et al. 2010) and folic acid (Ma et al. 2012; Pan et al. 2013; Xing et al. 2015; Yang et al. 2013) have been extensively studied as targeting ligands (Chen et al. 2014). Folic acid is suitable for tumor cells targeting because folate receptors are highly over-expressed on the surface of many tumor types. Xing et al. developed NPs coated with a folate-conjugated, light-responsive, and amphiphilic copolymer consisting of 1′-(2-methacryloxyethyl)-3′,3′-dimethyl-6-nitro-spiro (2H-1-benzopyran-2′,2′-in-doline) (SPMA), poly(ethylene glycol) methacrylate (MAPEG), and N-acryloxysuccinimide (NSA) units (Xing et al. 2015). Hydrophobic interactions between the alkyl chains of the copolymer and the lipophilic chains of the UCNP ligand permit the addition of a new capping layer on the UCNP surface placing the folate receptor at the nanohybrid periphery. The nanohybrid shows high emission efficiency, good dispersibility, stability in aqueous media, and is suitable for tumor targeting.

Furthermore, targeting can be through internalization of UNCPs by cells. The NPs ligand can play a crucial role, because it can control the UCNPs–cell interactions (Jin et al. 2011). Jin et al. have studied the effect of the charge of $NaYF_4$:Yb, Er UCNPs on the cellular uptake efficiency (determined by multiphoton microscopy), using PVP, PEI, and PAA as the organic capping. At the same conditions, positively charged UCNP@PEI NPs exhibited greatly enhanced cellular uptake in comparison with that of UCNP@PVP and UCNP@PAA (neutral and negative charged polymers, respectively) NPs, because the cell surface is usually negatively charged. So, the charge of the organic capping can improve the efficiency of the NPs internalization. Analogous results were obtained in the comparative study of $NaGdF_4$:Yb, Er UCNPs capped with PEG, PEI, and 6-aminocapronic acid (6AA) (Tsang et al. 2015b). Thus, the electrostatic interaction between $-NH_2$ groups on the UCNP@PEI

periphery and the cell membrane increased the efficiency in the cell uptake of the nanohybrid.

5.3.5.4 Sensing

UCNPs can be used to sense a physical stimulus or (bio)chemical species in their surroundings by the combination of the UCNP emission and organic capping functionality.

To date, studies of the suitability of UCNPs in physical sensing has mainly focused in temperature sensing (Chen et al. 2014; Hao et al. 2013). Although there are studies of their response to strain (Wisser et al. 2015), electrical (Hao et al. 2011; Huang and Hsieh 2009) and magnetic fields (Tikhomirov et al. 2009; G. Wang et al. 2011; Valiente et al. 2009), high radiation energy, and NIR-light, but this sensing makes use of their core intrinsic properties. Here we make special emphasis on the synergic effects between the organic capping and the UCNP in sensing. See recent reviews for more information regarding physical and (bio)chemical sensing with UCNPs (Christ and Schäferling 2015; González-Béjar and Pérez-Prieto 2015; Tsang et al. 2015a).

In thermometry of solids, there is no need to perform a modification on the organic coating of the synthesized NPs. However, it becomes crucial to prepare water-dispersible UCNPs with a nontoxic and biocompatible capping if they are going to be used for nanothermometry *in vivo* (Vetrone et al. 2010b). To that purpose *Vetrone* et al. used PEI-capped α-$NaYF_4$:Yb, Er NPs (Vetrone et al. 2010a). We have mentioned above an example of the cooperation between an UCNP and a polymer to sense temperature at values close to those of human body (Liras et al. 2014).

The organic ligand can play a key role in (bio)chemical sensing. Chemical sensing is usually based on UCNPs coated with a large number of photoactive molecules whose absorbance overlaps with some of the UCNP emission bands. Consequently, the sensing capacity is due to either inner filter effects or energy transfer processes from the UCNP to the capping molecule (e.g., a fluorophore within the polymeric coating). However, in biochemical sensing, the UCNPs are usually coated with receptors.

The starting point for (bio)chemical sensing with UCNPs is to meet the dispersibility requirement (either in organic or aqueous solvents) by making use of one of the strategies mentioned throughout this chapter (ligand exchange, layer by layer assembly, etc). In addition, the organic ligand must include either an organic molecule with sensing capabilities to the desired analyte (Hao et al. 2013) and the optical response must be proportional to the concentration of the analyte if the purpose is its quantification.

Figure 5.7 illustrates a nanohybrid where the on/off energy transfer between the UCNP (donor) and the fluorophore (acceptor) can be activated or deactivated upon recognition of the analyte. Many analytes (metal ions, gas molecules…) (Chen et al. 2014) have been recognized by using UCNP nanohybrids (Christ and Schäferling 2015; Hao et al. 2013).

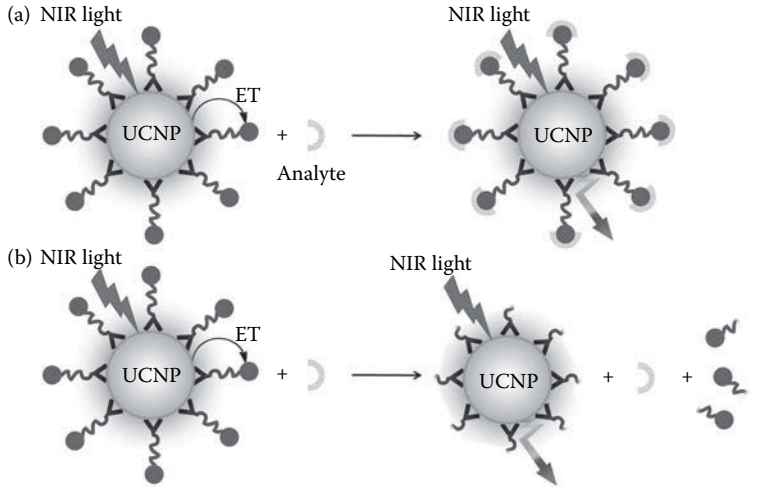

FIGURE 5.7
Analyte recognition via on/off energy transfer between UCNP (donor) and the fluorophore (acceptor). (a) Inhibition of the energy transfer through linking of the analyte to the acceptor. (b) Inhibition of the energy transfer because the analyte (usually an enzyme) cut off the bond between UCNP and fluorophore (acceptor).

Undoubtedly, pH reflects the concentration of protons in the medium and is a key target parameter in a broad range of applications such as life sciences, food and beverage processing, soil examination, and marine and pharmaceutical research (Wisser et al. 2015). Among the several detection methods available to detect pH changes, luminescent methods are recommended and most widely used (Wencel et al. 2014). Therefore, in this chapter we have selected pH sensing to illustrate possible designs of chemical sensors.

The aim is to avoid the drawbacks of commonly used pH indicators based on organic fluorophores, such as their photodegradation, photobleaching, and autofluorescence. In particular, water-dispersible UCNPs have been recently proven to be either pH-responsive (Wencel et al. 2014) or useful for pH measurement and sensing (Arppe et al. 2014; Esipova et al. 2012; Sun et al. 2009; Xie et al. 2012). The useful pH ranges reported for these systems are 6–11 for bromothymol blue/UCNPs (Esipova et al. 2012) and 6–10 for Nile blue derivative (ETH5418)/UCNPs (Sun et al. 2009) thin films, 2.5–7.5 for pHrodoTM Red dye/UCNPs (Xie et al. 2012), 5–9 for porphyrin/UCNPs (Arppe et al. 2014) and 5–8 for graphene oxide/UCNPs (Esipova et al. 2012). In addition, UCNP-based nanohybrids have been used for controlled release (Yan et al. 2014) and imaging guided PDT (Chen et al. 2014) using pH variations. Hexagonal $NaYF_4$:Yb, Er NPs ($NaYF_4$:Er^{3+}, Yb^{3+}) have been used for these purposes due to their superior UC efficiency (C. Wang et al. 2013).

Studies on the pH effect on UCNPs capped with azelaic acids ($HOOC(CH_2)_7COOH$) have proved that their emission is independent of the

pH in the range from 2 to 11 (Xie et al. 2012). By contrast, *N. Bogdan* et al. (Bogdan et al. 2011) have reported the influence of the pH on the red emission of naked $NaYF_4$:Yb, Er UCNPs. Nevertheless, two strategies have been proposed to make UCNPs pH sensitive based on the cooperativity between the organic capping and the UCNP. One of them is based on the stabilization of emissive NPs by multidentate pH-responsive polymers (Bogdan et al. 2012). The other one (useful for pH measurements) is based on the combination of UCNPs with a pH-probe (fluorescent or not; it can also be a nanomaterial) embedded in a silica shell or polymer matrix. The pH-dependent probe suffers a spectral shift according to the pH, and as a consequence the degree of overlap between its absorption and the UCNPs emission wavelengths varies, which results in a change in the ratio between the UCNPs emission bands and may also influence the energy transfer from the UCNPs to the acceptor (if the probe used can act as acceptor and not just as absorption filter) (Arppe et al. 2014; Liras et al. 2014; Sun et al. 2009). Gold nanoparticles (AuNPs) and UCNP can lead to pH sensitive systems (Arppe et al. 2014; Luo et al. 2013; Zhang et al. 2009). In some examples, the synergistic effect is due to the ligand on the AuNPs and it will not be discussed here (Zhang et al. 2009).

An example that perfectly shows the synergistic effect between the organic ligand and the UCNP for pH detection has been reported by *Zhao* et al. (Yan et al. 2014). They have designed a biocompatible pH sensitive film based on energy transfer between positively charged PEI-coated $NaYF_4$:Yb, Er UCNPs and negatively charged UCNPs and graphene oxide (GO). The interaction between them becomes stronger with increasing pH, since at acidic pHs values (e.g., pH = 5.00) the negative charge of the GO nanosheets decreases. Interestingly, the sensor film has been applied in real urine measurements.

In the case of biochemical sensing (or bioassay) the nanohybrids allow detection of biomolecules (antibody, immunoglobulin, etc.) in a solution and it can also be designed for the quantification of the biomolecule. The bioassay can be homogeneous or heterogeneous. The first assay consists in simply mixing the analytes and the sample and then carrying out an optical measurement, whereas the heterogeneous assay requires multiple steps in which the analytes are added usually in solution to a solid where the nanohybrid has been fixed. Later on, the solid is washed to ensure that only those analytes that have been recognized remain attached and separated at different points in the assay (Chen et al. 2014).

DNA/RNA analysis is of great interest in molecular biology, genetics, and molecular medicine (Zhang et al. 2006). *P. Zhang* et al. have synthesized UCNPs using a sandwich-type hybridization format composed by two shorter oligonucleotides with specific designed sequence to recognize the longer target oligonucleotide. One of the shorter oligonucleotides is covalently anchored to the nanoparticle surface and the other is used to attach a fluorophore which absorption spectrum overlaps with the emission spectrum of the NPs. Upon irradiation with NIR light and in the presence of the longer target oligonucleotide, emission of the fluorophore is observed due to

energy transfer from the UCNP to the fluorophore. This study demonstrates the high capacity of the nanohybrid to recognize DNA with a detection limit of 2.3 nM.

Aptamers are DNA/RNA molecules that are analogous to antibodies in their range of target recognition and in their high specificity (Wu et al. 2014). *Wu* et al. developed a highly stable, specific, and sensitive nanohybrid combining the multicolor properties of UCNPs with aptamers. Three different aptamers with specificity to *Staphylococcus aureus*, *Vibrio parahaemolyticus*, and *Salmonella typhimurium* bacteria were used. The specific recognition and high affinity of each nanohybrid for the target bacterium permit the detection of various types of bacteria coexisting in the same sample.

In addition, UCNPs conjugated with glycodendrimers have proved to recognize lectins via lanthanide resonance energy transfer (Bogdan et al. 2010). Poly(amidoamine) dendrimers were grafted to the surface of $NaGdF_4$:Yb, Er NPs, thus allowing the subsequent linking of carbohydrates to the dendrimers via a thiourea bond. The carbohydrates have an aromatic group in their structure, which plays two important roles. Whereas one of them recognizes proteins, such as lectin, via hydrophobic interactions, the other avoids the contact of water with the nanoparticle surface, which can quench the UCNP luminescence. The resulting UCNP nanohybrids possess excellent emission properties, which can be used to follow the recognition process of fluorophore-labeled Con A lectin by imaging.

5.3.5.5 Bioimaging

Fluorescence imaging is a noninvasive technique for real-time monitoring cells, biological processes, and morphological details in tissue and animals (Wu and Butt 2015). This technique is relevant for studying biological and pathological processes to provide important clues to the progression of several diseases (Dong et al. 2015). Bioimaging is applied in toxicity assessment, cellular and whole-body imaging, optical tomography, multimodal imaging, etc. (Ma and Ni 2015).

The NIR-response of UCNPs makes them particularly suitable for bioimaging applications due to the elimination of autofluorescence from biosamples (Kobayashi et al. 2009; Prodi et al. 2015), thus enabling high signal-to-noise ratio. In addition, UCNPs possess narrow emission bands that are advantageous for multicolor imaging (Cheng et al. 2011b), they show high photostability as compared to quantum dots and organic dyes, and they have low toxicity (Gnach et al. 2015). Interestingly, NIR light exhibits a remarkably deep penetration in tissues (Idris et al. 2009; Yu et al. 2009).

The organic capping plays a key role in the application of the UCNP in this field, since it can tune the emission properties of the nanoparticle and improve its stability and dispersibility in water or physiological media for *in vivo* studies (Chen et al. 2014). As mentioned in Section 5.3.5.4, surface properties can control the UCNP–cell interactions. Therefore, improved cellular

uptake without losing UC emission is desirable in cellular imaging. Three different polymers have been used to bind to the nanoparticle surface: PEG, PEI, and 6AA (Tsang et al. 2015b). UCL bioimaging in HeLa cells showed that PEI-capped UCNPs exhibited enhanced luminescence due to the presence of PEI amino groups, which have a high affinity for the cell membrane.

Lanthanide ions of the UCNPs can form complexes with cellular phosphate residues and this could be a biological hazard and interfere in the fluorescence of nanomaterials.

Ethylene diamine-tetra methylene phosphonic acid (EDTMP) is a compound with four C-PO(OH)$_2$ groups that can anchor to the surface of UCNPs with high affinity (R. Li et al. 2015). Consequently, EDMPT can be used to protect the UCNP and prevent its complexation to cellular phosphates, thus preserving its fluorescence.

AA-capped $NaGdF_4$:Yb, Tm, Er (UCNP@AA) NPs were developed to achieve whole body bioimaging of a mouse (Zhou et al. 2010). After 40 min of an intravenous injection of a solution containing UCNP@AA, an upconvertion luminescence (UCL) signal was detected and an image of the whole body was obtained. The presence of AA on the nanoparticle surface conferred good water dispersibility to the UCNP as well as low cytotoxicity for the biological system, therefore the UCNP@AA nanohybrid was suitable for bioimaging.

Another interesting example of the ligand role is tuning the multicolor UC emission of $NaYF_4$:Yb, Er by adjusting the molar ratio of two coordinating ligands on the surface of UCNPs (Niu et al. 2010). NPs were synthesized using a mixture of octadecylamine and oleamide via a thermolysis procedure. The increase of the oleamide/octadecylamine molar ratio caused the color emission output to change from green to red. Multicolored UCNPs are important for multiplexed bioimaging because they enable simultaneous monitoring of the interaction between multiple proteins or cells within an organism and a panel of sub-level parts of an organ (Dong et al. 2015; Zhou et al. 2015).

5.3.5.6 Therapy

As explained in Section 5.3.5.5, UCNPs seem to be biologically friendly (Gnach et al. 2015) and are of a noninvasive nature (Chen et al. 2014). These qualities make them suitable for theranostic applications, since they can integrate imaging and therapy capacities into a single platform and therefore they are useful for diagnosis, drug delivery, and monitoring of therapeutic response (Xie et al. 2010). The key features to consider when selecting a luminescent particle for therapy are the absorption wavelength, the emission wavelength, and the size of the particle and the capping ligand. UCNPs are used for two purposes in therapeutic applications. One, they convert NIR to UV–Vis, which extends the operating range of therapeutic agents thanks to energy transfer processes or induced photorelease (Zhou et al. 2015). And

two, as discussed in the previous section, they can be used as probes to monitor (bio)chemical changes and they can be employed to monitor the distribution and metabolism of drugs (Zhou et al. 2015). In this section, we discuss a number of notable therapies in the field, which are: PDT, photo thermal therapy (PTT), and chemotherapy, and a combination of them all.

5.3.5.6.1 Photodynamic Therapy

PDT is a noninvasive cancer treatment based on selective delivery/administration of a PS, which upon selective excitation is capable of generating singlet oxygen (type II mechanism) and/or other reactive oxygen species (ROS) (type I mechanism), causing tumoral cells apoptosis and/or necrosis exclusively in the illuminated area and its surroundings (Brown et al. 2004; Dougherty 1993). To date, most PSs used for this purpose are organic molecules or complexes that absorb visible light and are soluble in aqueous solutions. Unfortunately, they tend to aggregate and they lose their photochemical activity upon prolonged illumination (Ideat et al. 2005). Even worse, the penetration of visible light through tissues is very limited as compared to NIR. So it is advantageous to use UCNPs to absorb NIR light and be able to transfer this energy to a PS. With regard to the excitation wavelength, 975 and 920 nm are the most used to excite Yb^{3+} in the UCNPs (Chen et al. 2013; Vetrone et al. 2010b), though other designs using 808 nm have recently been reported (e.g., rose bengal (RB)-capped $NaYF_4$:Yb,Ho@$NaYF_4$:Nd@$NaYF_4$ UCNPs (Dong et al. 2015; Wang et al. 2015). As illustrated in previous sections (e.g., sensing), a pre-requisite for the Energy transfer (ET) process is that the surrounding chromophore (a PS in this particular case) absorbs light where the UCNPs emit. Here we emphasize the photophysical and photochemical events that take place after excitation of the PS through the ET process to lead eventually to reactive species that cause tumoral cells death. Figure 5.8 shows a simplified representation of the process: energy transfer from the UCNP to the PS leads to the PS singlet-excited state (^{1}PS) that would lead to its triplet excited state (^{3}PS) by intersystem crossing. Then, singlet oxygen (and/or other ROS such as hydroxyl radicals or superoxide anion radical) would be generated by triplet–triplet energy transfer (or electron transfer) from the (^{3}PS) to oxygen in the GS.

The high surface/volume ratio of the NIR-responsive UCNPs combined with the capacity of their surface and ligands to establish stabilizing binding interactions with the PDT PS evidences the cooperative effect in the organic-coated UCNP system. Undoubtedly, an ideal UCNP–PS nanohybrid for PDT would be a nontoxic and biocompatible, stable, water-dispersible, small-sized (able to permeate the cell membrane) nanohybrid with a large loading of a PS. It is also desirable to avoid leaching of the PS into the living system.

There are several designs to load water-dispersible UCNPs, usually $NaYF_4$:Yb(Er and/or Tm), with a PS or combination of PSs to maximize the overlap with the UCNPs emission (Idris et al. 2012). Some PSs have been

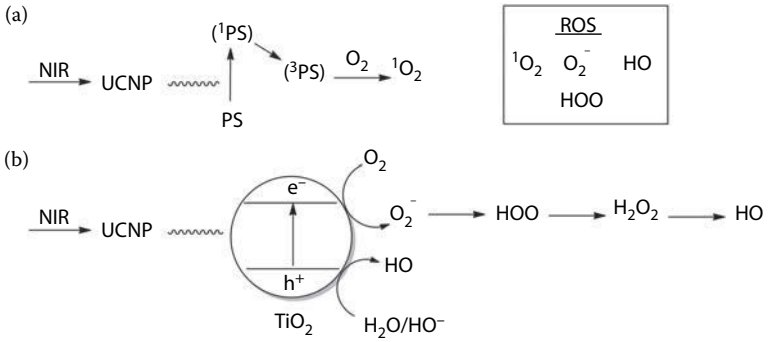

FIGURE 5.8
Photosensitized generation of singlet oxygen (a) and other ROS (b).

embedded in polymeric shells around the UCNP core (e.g., ZnPc (Cui et al. 2013), pyropheophorbide a (Zhou et al. 2012), monomalonic fullerene (X. Liu et al. 2013), and Ce6 (Cheng et al. 2011a; Park et al. 2012)).

In addition, PSs, such as rose bengal (RB), Zn(II) phthalocyanine (ZnPc), and Bodipy derivatives have been covalently bonded to $NaYF_4$:RE UCNP scapped with 2-aminoethyl dihydrogen phosphate (Liu et al. 2012), PAAm (Xia et al. 2014), and PEI (Topel et al. 2014), respectively.

Moreover, it has been recently demonstrated that carboxy-functionalized PSs, such as a carboxybodipy (Bodipy-COOH), (González-Béjar et al. 2014) and carboxyphthalocyanine zinc (ZnPc-COOH) (M. Wang et al. 2014) can be grafted to the UCNP surface to lead to nanohybrids able to generate singlet oxygen efficiently. Singlet oxygen is one of the possible ROS that can lead to tumor cell killing.

A novel series of $NaYF_4$:Yb,Tm@TiO_2 nanosystems has been recently designed for *in vivo* tumor PDT (Lucky et al. 2015). In order to make this nanosystem water-dispersible, the nanosystem was coated with a polymeric shell (PEG derivative). The mechanism associated to ROS for TiO_2 (Hoffmann et al. 1995; Linsebigler et al. 1995; Oppenlander 2003) is activated after NIR excitation of the UCNP followed by energy transfer to TiO_2. Figure 5.8 illustrates the charge separation (electron/holepair) induced upon TiO_2 irradiation (Anpo and Kamat 2010; García et al. 2009; Khataee and Fathinia 2013). These electron–hole pairs can recombine and the charge carriers can competitively migrate to the TiO_2 surface, eventually leading to hydroxyl free radicals in the presence of water and oxygen (Furube et al. 1999). The *in vivo* tumor PDT treatment with $NaYF_4$:Yb,Tm@TiO_2 proved efficient in delaying the tumor growth.

Most of the just described nanosystems have been tested for PDT *in vitro* with diverse tumor cell lines, but a few of them have been successfully tested *in vivo* (mice have been used for this purpose). Generally, the tumor of the mice is treated with the nanosystem and NIR-light and its evolution

is compared with that of other tumors under control treatment conditions (i.e., saline solution and NIR-irradiation; no irradiation and the nanosystem) in order to make sure that the volume of the tumor decreases exclusively due to UCNP/NIR-light combination. In some cases, the nanosystem is also loaded with folate to increase the tumor-selectivity since cancer cells overexpress folate receptor. The above-mentioned PDT nanocomposites that comprise one type of PS and have been tested *in vivo* are discussed below.

The first demonstration of NIR light-induced *in vivo* PDT of cancer with $NaYF_4$:Yb,Er UCNPs loaded with Ce6 as PS was reported by Liu et al. (Furube et al. 1999). In this nanosystem, Ce6 absorbs red emission of Er^{3+} and it is intercalated between the lipophilic chains of the interdigitated area between the oleate capping the UCNP surface and a polymeric coating (Figure 5.5). Two important findings were proven in this report. First, the tumor volume of mice treated with Ce6-functionalized UCNPs and NIR light irradiation was much smaller (about 60%) than that of mice treated with saline and visible light irradiation. Secondly, tissue penetration depth observed by NIR irradiation was much deeper than that of visible illumination. Interestingly, later on the authors developed charge-reversible $NaYF_4$:Mn,Yb,Er UCNPs loaded with Ce6 for pH-sensitive *in vivo* PDT (Park et al. 2012). These UCNPs emit strong red light emission at ca. 660 nm under 980 nm NIR that can be absorbed by the PS to generate singlet oxygen. The novelty here is due to the use of a pH-sensitive polymer that improves the cancer cell killing efficacy in a slightly acidic environment; it has to be taken into account that tumor extracellular environment is slightly acidic (pH 6.5–6.8). The nanosystem is negatively charged in neutral and alkaline environments but becomes positively charged under slightly acidic conditions. This enhances the cellular uptake of the NPs due to a highly favorable interaction with negatively charged cell membranes. This example combines several synergistic effects that allow pH sensing and singlet oxygen generation *in vivo* under NIR illumination.

Cui et al. designed $NaYF_4$:Yb,Er UCNPs coated with folate-modified chitosan to anchor PS molecules of ZnPc in order to realize *in vivo* targeted deep-tissue PDT and a tumor inhabitation ratio of 50% was achieved (Cui et al. 2012, 2013).

In 2014, ZnPc-LiYF_4:Yb, Er (Xia et al. 2014) and 5-aminolevulinic acid-capped $NaYF_4$:Yb,Er@ CaF_2 NPs (M. Wang et al. 2014) were also constructed and proven to be successful.

Another example of application in tumor targeted imaging and PDT is that of UCNPs co-loaded with aminophenylboronic acid (APBA) and hyaluronated fullerene (HAC_{60}) (X. Wang et al. 2014). APBA was used as a stabilizer in the synthesis and as a functional ligand for targeting bioimaging, whereas HAC_{60} was used as an acceptor to generate singlet oxygen. The two ligands on the surface of the NPs made possible the quenching of UC emission via energy transfer processes. Also, uptake of the nanohybrid by PC12 cancer cells was dramatically enhanced compared with HAC_{60} without UCNPs.

Therefore, the synergistic effect between the core NPs and the capping ligands led to a nanohybrid with two color fluorescent signals, high specificity, high cell uptake, and improved PDT.

5.3.5.6.2 Photothermal Therapy

In PTT treatment, the tumor loaded with the proper agent (e.g., NPs) is exposed to an excitation source. This light is absorbed by the agent and converted it into heat (local hyperthermia), thus killing cancer cells (e.g., the temperature of the tissue raises and, as a consequence, cancerous cells are ablated) (Philipp et al. 1995).

To date, AuNPs (Kennedy et al. 2011), organic dyes, graphene oxides, and quantum dots have shown to be effective agents for PTT. Although UCNPs are relevant due to their capacity to absorb NIR light, they require the presence of the above-mentioned agents to be used in PTT and the only role of the organic capping is to provide hydrophilicity to the nanosystem. For example, PEG-modified $NaYF_4$:Yb,Er@ Fe_3O_4@Au nanohybrids have been used for dual-mode imaging guided PTT (Cheng et al. 2011a; Cheng et al. 2012). In this nanocomposite, PEG provides water dispersibility, $NaYF_4$:Yb,Er generates UC emissions, Fe_3O_4 is responsible for the T2-weighted Magnetic resonance imaging (MRI), and the Au shell converts NIR light into heat. After intravenous injection of the nanocomposite, the temperature at the tumors surface increases to ~50°C, as compared to ~38°C for irradiated tumors in the absence of the nanocomposites.

However, nanohybrids comprising UCNPs and functional organic ligands are of interest for combined PTT/PDT therapy. An interesting system is that in which PAAm-capped $NaYF_4$:Yb,Er,Tm@$NaYF_4$ UCNPs (UCNPs-NH_2) was coupled to functionalized graphene oxide (NGO-COOH) and ZnPc molecules were adsorbed on the GO surface (Y. Wang et al. 2013). The efficiency in the cancer cell death increased by using two lasers (808 nm for PTT, 630 nm for PDT) simultaneously to irradiate the nanocomposites that had been up-taken by the cancer cells (Figure 5.9).

5.3.5.7 Drug Delivery and Chemotherapy

Chemotherapy is the main technique to cure diseases like cancer with the disadvantage to control the local effective therapeutic concentration, causing cytotoxicity at high concentrations (Dong et al. 2015). In general, UCNP-assisted chemotherapeutic processes fall into two categories: (a) UCL-guided monitoring of the degree of drug release (Dong et al. 2015) and (b) NIR-triggered drug release based on UCNPs (Figure 5.10) (Wu and Butt 2015).

In addition, UCNPs act as versatile nano-transducers converting NIR light to light of shorter wavelengths and, consequently, NIR-light excitation can eventually induce changes in close-lying molecules which absorb at shorter wavelengths and/or can induce their release by photo-cleavage. These NIR light-induced processes are of particular interest in biological samples for

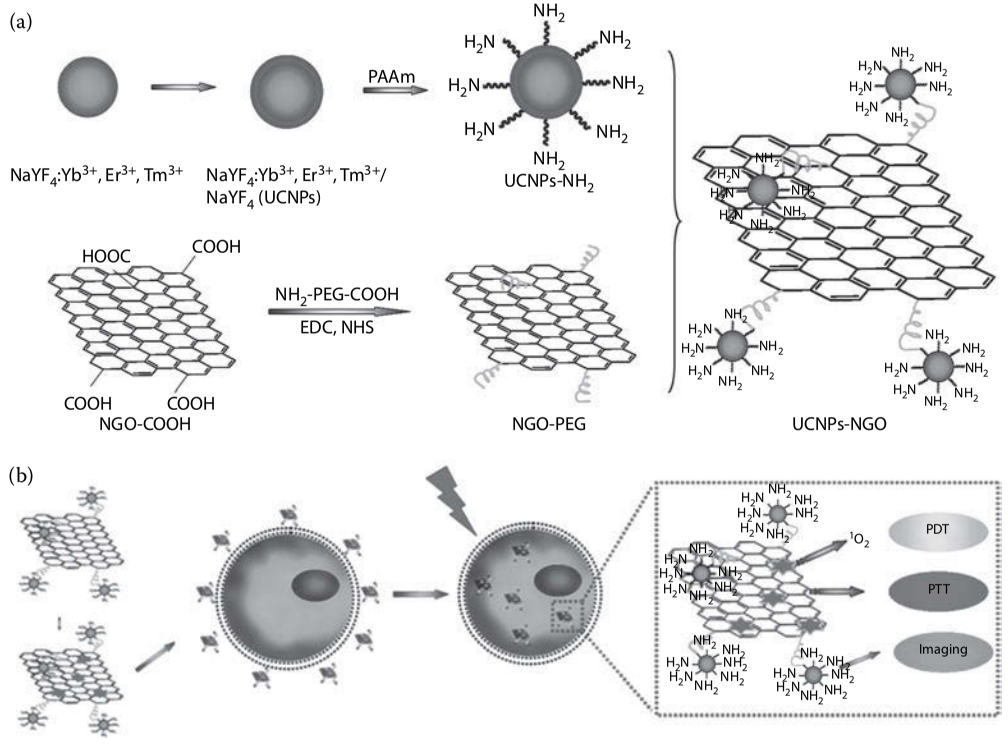

FIGURE 5.9
(a) Schematic illustration of the synthetic procedure for UCNPs–NGO: Numbers of core–shell structured UCNPs being covalently grafted with NGO via bifunctional PEG; (b) Schematic illustration of UCNPs–NGO/ZnPc as a multifunctional theranostic nanoplatform for cancer treatment. (Reprinted from *Biomaterials*, 34/31, Wang, Y., H. Wang, D. Liu, S. Song, X. Wang, H. Zhang, Graphene oxide covalently grafted UCNPs for combined NIR mediated imaging and photothermal/photodynamic cancer therapy, 7715–7724, Copyright 2013, with permission from Elsevier.)

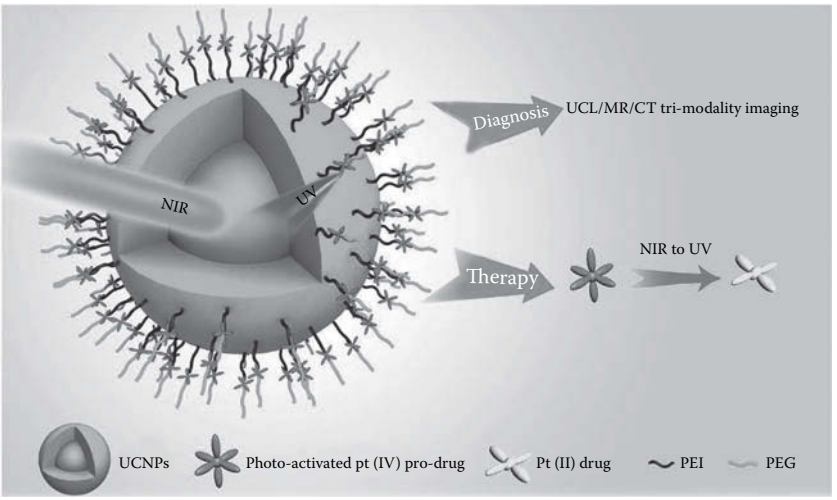

FIGURE 5.10
Schematic illustration of the characterization of UCNP–DPP–PEG NPs and their use for diagnosis and photorelease. (Adapted from Dai, Y., H. Xiao, J. Liu et al. 2013. In vivo multimodality imaging and cancer therapy by NIR light-triggered trans-platinum pro-drug-conjugated upconverison NPs. Journal of the American Chemical Society 135 (50):18920–18929.). Copyright 2015 American Chemical Society.)

remote-control release of caged compounds, such as drugs (Yang et al. 2015), since their light-dependence determines where and when a process is initiated (Idris et al. 2015).

An example is that occurring after NIR excitation of $NaYF_4$:Yb, Er NPs capped with PAA in the presence of eosin Y (photoinitiator that exhibits a strong absorption band between 460 and 540 nm), *N*-vinylpyrrolidone (NVP), and Poly(ethylene-glycol)-diacrylate (PEGDA). Energy transfer from the UCNP to eosin Y generates free radicals which initiate the polyaddition reaction of the carbon–carbon double bond of NVP and PEGDA (Xiao et al. 2013) to form cross-linked hydrogels. Progressive light irradiation of the system eventually leads to UCNP–PEGDA hybrid microspheres due to the aggregation of the NPs via hydrogen bonding between the PAA-capping and the PEGDA hydrogel. These hybrid microspheres can be loaded with ZnPc by hydrophobic interactions to give rise to a system with a high efficiency in singlet oxygen generation (Xiao et al. 2013).

In addition, UCNP luminescence can be absorbed by close-lying molecules, eventually inducing drug-release by photocleavage. For example, NIR laser light excitation of UCNPs encapsulated in UV light-degradable polymer particles causes the degradation of the polymer into its monomers by inducing cleavage of a protective group (Viger et al. 2013). This strategy also proved successful to control the release of coumarin 153 (C153) remotely by irradiating at 980 nm.

Moreover, PEG-capped (Ruggiero et al. 2015) and PEI-capped (Dai et al. 2013) β-$NaYF_4$:Yb,Tm@$NaGdF_4$:Yb NPs were covalently conjugated to a platinum (IV) antitumor drug, namely the *trans,trans,trans*-[$Pt(N_3)_2(NH_3)(py)(O_2CCH_2CH_2COOH)_2$] (DPP) pro-drug (Figure 5.10). An added layer of PEG improved the stability and biocompatibility of the nanohybrid. The synergistic effect between the organic capping and the nanoparticle core allowed the selective drug delivery induced by NIR excitation (30 min of irradiation led to 48% of the drug delivery) (Dai et al. 2013). These UCNP nanohybrids were used as multifunctional drug delivery systems which combine NIR-activated platinum pro-drug delivery and UCL/magnetic resonance/computer tomography trimodality imaging.

The activity of proteins in protein-based therapies with UCNPs can be modified as a consequence of their covalent attachment to the UCNPs and therefore, it would be advantageous if the delivery of the nanohybrid was followed by the protein release. In this way, a DNA-mediated hierarchical hollow UCNP has been developed (Zhou et al. 2014). Hollow UCNPs were functionalized with 3-aminopropyltriethoxysilane (APTES) to afford UCNPs-NH_2, and then a spiropyran dye (SP-COOH) was conjugated. When the SP molecule is irradiated with UV-light it isomerizes to the merocyanine (MC) form. This isomerization is reversible with visible light. The authors demonstrated that positively charged MC-functionalized UCNPs allow the electrostatic interaction with negatively charged proteins, such as β-galactose. So, after irradiation at 980 nm, hollow UCNPs transform the NIR light into visible light, which is absorbed by MC, reverting back to the neutral SP form. Hence, the trapped proteins are released to the solution (70 wt% in 720 min after NIR exposure) (Zhou et al. 2014).

5.4 Summary

The UCNPs can be capped with a variety of organic compounds which possess an anchoring group to attach to the nanoparticle surface and can also contain functional molecules and/or functional groups. The combination of both components can be used to create smart NIR-responsive nanosystems with many biological and nanotechnological applications. In this chapter, we have tried to select typical examples to visualize how the nanoparticle and the organic capping work together to provide the desired functionality; additional examples can be found in related literature reviews. (Auzel 2004), (Wolfbeis 2015), (Idris et al. 2015), (Wu et al. 2015), (Zhou et al. 2015), (Yang et al. 2015), (Li et al. 2015), (Sedlmeier and Gorris 2015), (Prodi et al. 2015), (Naccache et al. 2015), (González-Béjar and Pérez-Prieto 2015), (Gnach et al. 2015), (Dong et al. 2015), (Christ and Schäferling 2015), (Cheng and Lin 2015), (Chan et al. 2015), (Tsang et al. 2015a), (G. Chen et al.

2015); (Park et al. 2015), (Chan 2015), (H. Chen et al. 2015), (Bünzli 2015), (Kerr De La Rica 2015), (Tu et al. 2015), (Wu and Butt 2015), (Ramasamy et al. 2014), (Muhr et al. 2014), (Gai et al. 2014), (Dacosta et al. 2014), (Chen et al. 2014), (Gu et al. 2013), (Chen et al. 2013), (Y. Liu et al. 2013), (Gnach and Bednarkiewicz 2012), (Chen et al. 2012), (Wang et al. 2011), (Haase and Schäfer 2011), (Fischer et al. 2011), (Li and Lin 2010).

References

Anpo, M. and P. V. Kamat. 2010. *Enviromentally Begin Photocatalysts. Applications of Titanium Oxide-Based Materials*. New York: Springer Science Business Media, LCC.

Arppe, R., I. Hyppanen, N. Perala et al. 2015. Quenching of the upconversion luminescence of $NaYF_4$:Yb^{3+},Er^{3+} and $NaYF_4$:Yb^{3+},Tm^{3+} nanophosphors by water: The role of the sensitizer Yb^{3+} in non-radiative relaxation. *Nanoscale* 7 (27):11746–11757.

Arppe, R., T. Nareoja, S. Nylund et al. 2014. Photon upconversion sensitized nanoprobes for sensing and imaging of pH. *Nanoscale* 6 (12):6837–6843.

Auzel, F. 2004. Upconversion and anti-stokes processes with f and d ions in solids. *Chem. Rev.* 104 (1):139–174.

Bogdan, N., E. M. Rodriguez, F. Sanz-Rodriguez et al. 2012. Bio-functionalization of ligand-free upconverting lanthanide doped nanoparticles for bio-imaging and cell targeting. *Nanoscale* 4 (12):3647–3650.

Bogdan, N., F. Vetrone, G. A. Ozin et al. 2011. Synthesis of ligand-free colloidally stable water dispersible brightly luminescent lanthanide-doped upconverting nanoparticles. *Nano Lett.* 11 (2):835–840.

Bogdan, N., F. Vetrone, R. Roy et al. 2010. Carbohydrate-coated lanthanide-doped upconverting nanoparticles for lectin recognition. *J. Mater. Chem.* 20 (35):7543.

Boyer, J.-C., M.-P. Manseau, J. I. Murray et al. 2010. Surface modification of upconverting $NaYF_4$ nanoparticles with PEG-Phosphate ligands for NIR (800 nm) biolabeling within the biological window. *Langmuir* 26 (2):1157–1164.

Boyer, J.-C. and F. C. J. M. Van Veggel. 2010. Absolute quantum yield measurements of colloidal $NaYF_4$: Er^{3+}, Yb^{3+} upconverting nanoparticles. *Nanoscale* 2 (8):1417–1419.

Brown, S. B., E. A. Brown, and I. Walker. 2004. The present and future role of photodynamic therapy in cancer treatment. *Lancet Oncol.* 5 (8):497–508.

Bünzli, J.-C. G. 2015. Lanthanide light for biology and medical diagnosis. *J. Lumin.* doi: http://dx.doi.org/10.1016/j.jlumin.2015.07.033.

Cui, S., H. Chen, H. Zhu et al. 2012. Amphiphilic chitosan modified upconversion nanoparticles for in vivo photodynamic therapy induced by near-infrared light. *J. Mater. Chem.* 22:4861–4873.

Cui, S., D. Yin, Y. Chen et al. 2013. In vivo targeted deep-tissue photodynamic therapy based on near-infrared light triggered upconversion nanoconstruct. *ACS Nano* 7 (1):676–688.

Chan, E. M. 2015. Combinatorial approaches for developing upconverting nanomaterials: High-throughput screening, modeling, and applications. *Chem. Soc. Rev.* 44 (6):1653–1679.

Chan, E. M., E. S. Levy, and B. E. Cohen. 2015. Rationally designed energy transfer in upconverting nanoparticles. *Adv. Mater.* 27 (38):5753–5761.

Chen, G., H. Agren, T. Y. Ohulchanskyy et al. 2015. Light upconverting core–shell nanostructures: Nanophotonic control for emerging applications. *Chem. Soc. Rev.* 44 (6):1680–1713.

Chen, G., T. Y. Ohulchanskyy, R. Kumar et al. 2010. Ultrasmall monodisperse $NaYF_4$:Yb^{3+}/Tm^{3+}nanocrystals with enhanced near-Infrared to near-infrared upconversion photoluminescence. *ACS Nano* 4 (6):3163–3168.

Chen, G., H. Qiu, P. N. Prasad et al. 2014. Upconversion nanoparticles: Design, nanochemistry, and applications in theranostics. *Chem. Rev.* 114 (10):5161–5214.

Chen, G., C. Yang, and P. N. Prasad. 2013. Nanophotonics and nanochemistry: Controlling the excitation dynamics for frequency up- and down-conversion in lanthanide-doped nanoparticles. *Acc. Chem. Res.* 46 (7):1474–1486.

Chen, H., D. Shi, Y. Wang et al. 2015. The advances in applying inorganic fluorescent nanomaterials for the detection of hepatocellular carcinoma and other cancers. *RSC Adv.* 5 (97):79572–79584.

Chen, J. and J. X. Zhao. 2012. Upconversion nanomaterials: Synthesis, mechanism, and applications in sensing. *Sensors* 12 (3):2414–2435.

Cheng, L., K. Yang, Y. Li et al. 2011a. Facile preparation of multifunctional upconversion nanoprobes for multimodal imaging and dual-targeted photothermal therapy. *Angew. Chem. Int. Ed.* 50:7385–7390.

Cheng, L., K. Yang, Y. Li et al. 2012. Multifunctional nanoparticles for upconversion luminescence/MR multimodal imaging and magnetically targeted photothermal therapy. *Biomaterials* 33 (7):2215–2222.

Cheng, L., K. Yang, M. Shao et al. 2011b. Multicolor in vivo imaging of upconversion nanoparticles with emissions tuned by luminescence resonance energy transfer. *J. Phys. Chem.* C 115 (6):2686–2692.

Cheng, Z. and J. Lin. 2015. Synthesis and application of nanohybrids based on upconverting nanoparticles and polymers. *Macromol. Rapid Comm.* 36 (9):790–827.

Christ, S. and M. Schäferling. 2015. Chemical sensing and imaging based on photon upconverting nano- and microcrystals: A review. *Methods Appl. Fluoresc.* 3 (3):034004.

Dacosta, M. V., S. Doughan, Y. Han et al. 2014. Lanthanide upconversion nanoparticles and applications in bioassays and bioimaging: A review. *Anal. Chim. Acta* 832:1–33.

Dai, Y., H. Xiao, J. Liu et al. 2013. In vivo multimodality imaging and cancer therapy by near-infrared light-triggered trans-platinum pro-drug-conjugated upconversion nanoparticles. *J. Am. Chem. Soc.* 135 (50):18920–18929.

Dong, A., X. Ye, J. Chen et al. 2011. A generalized ligand-exchange strategy enabling sequential surface functionalization of colloidal nanocrystals. *J. Am. Chem. Soc.* 133 (4):998–1006.

Dong, B., S. Xu, J. Sun et al. 2011. Multifunctional $NaYF_4$:Yb^{3+},Er^{3+} Integration of upconversion imaging and photothermal therapy. *J. Mater. Chem.* 21 (17):6193–6200.

Dong, H., S. R. Du, X. Y. Zheng et al. 2015. Lanthanide nanoparticles: From design toward bioimaging and therapy. *Chem. Rev.* 115 (19):10725–10815.

Dougherty, T. J. 1993. Photodynamic therapy. *Photochem. Photobiol.* 58 (6):895–900.

Esipova, T. V., X. Ye, J. E. Collins et al. 2012. Dendritic upconverting nanoparticles enable in vivo multiphoton microscopy with low-power continuous wave sources. *Proc. Natl. Acad. Sci.* 109 (51):20826–20831.

Friedman, A. D., S. E. Claypool, and R. Liu. 2013. The smart targeting of nanoparticles. *Curr. Pharm. Des.* 19 (35):6315–6329.

Fischer, L. H., G. S. Harms, and O. S. Wolfbeis. 2011. Upconverting nanoparticles for nanoscale thermometry. Angew. *Chem., Int. Ed.* 50 (20):4546–4551.

Francés-Soriano, L., M. González-Béjar, and J. Pérez-Prieto. 2015. Cucurbit[n]uril-capped upconversion nanoparticles as highly emissive scaffolds for energy acceptors. *Nanoscale* 7 (12):5140–5146.

Furube, A., T. Asahi, H. Masuhara et al. 1999. Charge carrier dynamics of standard TiO_2 catalysts revealed by femtosecond diffuse reflectance spectroscopy. *J. Phys. Chem.* B 103 (16):3120–3127.

Gai, S., C. Li, P. Yang et al. 2014. Recent progress in rare earth micro/nanocrystals: Soft chemical synthesis, luminescent properties, and biomedical applications. *Chem. Rev.* 114 (4):2343–2389.

García, J. C., J. I. Simionato, A. E. C. Da Silva et al. 2009. Solar photocatalytic degradation of real textile effluents by associated titanium dioxide and hydrogen peroxide. *Sol. Energy* 83:316–322.

Gnach, A. and A. Bednarkiewicz. 2012. Lanthanide-doped up-converting nanoparticles: Merits and challenges. *Nano Today* 7 (6):532–563.

Gnach, A., T. Lipinski, A. Bednarkiewicz et al. 2015. Upconverting nanoparticles: Assessing the toxicity. *Chem. Soc. Rev.* 44 (6):1561–1584.

González-Béjar, M., M. Liras, L. Francés-Soriano et al. 2014. NIR excitation of upconversion nanohybrids containing a surface grafted Bodipy induces oxygen-mediated cancer cell death. *J. Mater. Chem.* B 2 (28):4554–4563.

González-Béjar, M. and J. Pérez-Prieto. 2015. Upconversion luminescent nanoparticles in physical sensing and in monitoring physical processes in biological samples. *Methods Appl. Fluoresc.* 3 (4):042002.

Gu, Z., L. Yan, G. Tian et al. 2013. Recent advances in design and fabrication of upconversion nanoparticles and their safe theranostic applications. *Adv. Mater.* 25 (28):3758–3779.

Guo, J., F. Ma, S. Gu et al. 2012. Solvothermal synthesis and upconversion spectroscopy of monophase hexagonal $NaYF_4$:Yb^{3+}/Er^{3+} nanosized crystallines. *J. Alloy. Compd.* 523:161–166.

Haase, M. and H. Schäfer. 2011. Upconverting nanoparticles. *Angew Chem Int Ed* 50 (26):5808–5829.

Hao, J., Y. Zhang, and X. Wei. 2011. Electric-induced enhancement and modulation of upconversion photoluminescence in epitaxial $BaTiO_3$:Yb/Er thin films. *Angew. Chem., Int. Ed.* 50 (30):6876–6880.

Hao, S., G. Chen, and C. Yang. 2013. Sensing using rare-earth-doped upconversion nanoparticles. *Theranostics* 3 (5):331–345.

Heer, S., K. Kömpe, H. U. Güdel et al. 2004. Highly efficient multicolour upconversion emission in transparent colloids of lanthanide-doped $NaYF_4$ nanocrystals. *Adv. Mater.* 16 (23–24):2102–2105.

Hoffmann, M. R., S. T. Martin, W. Choi et al. 1995. Environmental applications of semiconductor photocatalysis. *Chem. Rev.* 95 (1):69–96.

Huang, T. C. and W. F. Hsieh. 2009. Er-Yb codoped ferroelectrics for controlling visible upconversion emissions. *J. Fluoresc.* 19:511–516.

Ideat, R., F. Tasaka, W.-D. Jang. et al. 2005. Nanotechnology-based photodynamic therapy for neovascular disease using a supramolecular nanocarrier loaded with a dendritic photosensitizer. *Nano Lett.* 5 (12):2426–2431.

Idris, N. M., M. K. Gnanasammandhan, J. Zhang et al. 2012. In vivo photodynamic therapy using upconversion nanoparticles as remote-controlled nanotransducers. *Nature Med.* 18 (10):1580–1585.

Idris, N. M., M. K. G. Jayakumar, A. Bansal et al. 2015. Upconversion nanoparticles as versatile light nanotransducers for photoactivation applications. *Chem. Soc. Rev.* 44 (6):1449–1478.

Idris, N. M., Z. Li, L. Ye et al. 2009. Tracking transplanted cells in live animal using upconversion fluorescent nanoparticles. *Biomaterials* 30 (28):5104–5113.

Jin, J., Y-Juan Gu, Cornelia Wing-Yin Man et al. 2011. Polymer-coated $NaYF_4$:Yb^{3+}, Er^{3+} upconversion nanoparticles for charge-dependent cellular imaging. *ACS Nano* 5 (10):7838–7847.

Kennedy, L. C., Bickford L. R., Lewinski N. A. et al. 2011. A new era for cancer treatment: Gold-nanoparticle-mediated thermal therapies. *Small* 7 (2):169–183.

Kerr, C. A. and R. De La Rica. 2015. Photoluminescent nanosensors for intracellular detection. *Anal. Methods* 7 (17):7067–7075.

Khataee, A. R. and M. Fathinia. 2013. New and future developments in catalysis: Nanoparticle catalysis by surface plasmon. In *Recent Advances in Photocatalytic Processes by Nanomaterials*, edited by Steven L. Sun, 267–288. United Kingdom: Elsevier Science Ltd.

Kobayashi, H., N. Kosaka, M. Ogawa et al. 2009. In vivo multiple color lymphatic imaging using upconverting nanocrystals. *J. Mater. Chem.* 19 (36):6481.

Lei, L., J. Zhou, J. Zhang et al. 2015. The use of zinc ions to control the size of Yb/Er:$KMnF_3$ nanocrystals with single band emission. *CrystEngComm* 17 (44):8457–8462.

Li, C. and J. Lin. 2010. Rare earth fluoride nano-/microcrystals: Synthesis, surface modification and application. *J. Mater. Chem.* 20 (33):6831.

Li, R., Z. Ji, J. Dong et al. 2015. Enhancing the imaging and biosafety of upconversion nanoparticles through phosphonate coating. *ACS Nano* 9 (3):3293–3306.

Li, X., F. Zhang, and D. Zhao. 2015. Lab on upconversion nanoparticles: Optical properties and applications engineering via designed nanostructure. *Chem. Soc. Rev.* 44 (6):1346–1378.

Li, Z. and Y. Zhang. 2008. An efficient and user-friendly method for the synthesis of hexagonal-phase $NaYF_4$:Yb, Er/Tm nanocrystals with controllable shape and upconversion fluorescence. *Nanotechnology* 19 (34):345606.

Liang, S., X. Zhang, Z. Wu et al. 2012. Decoration of up-converting NaYF4:Yb,Er(Tm) nanoparticles with surfactant bilayer. A versatile strategy to perform oil-to-water phase transfer and subsequently surface silication. *CrystEngComm* 14 (10):3484.

Linsebigler, A. L., G. Lu, and J. T. Yates Jr. 1995. Photocatalysis on TiO_2 Surfaces: Principles, mechanisms, and selected results. *Chem. Rev.* 95:735–758.

Liras, M., M. González-Béjar, E. Peinado et al. 2014. Thin amphiphilic polymer-capped upconversion nanoparticles: Enhanced emission and thermoresponsive properties. *Chem. Mater.* 26 (13):4014–4022.

Liu, J., W. Bu, L. Pan et al. 2013. NIR-triggered anticancer drug delivery by upconverting nanoparticles with integrated azobenzene-modified mesoporous silica. *Angew. Chem. Int. Ed.* 52 (16):4375–4379.

Liu, K., X. Liu, Q. Zeng et al. 2012. Covalently assembled NIR nanoplatform for simultaneous fluorescence imaging and photodynamic therapy of cancer cells. *ACS Nano* 6 (5):4054–4062.

Liu, Q., C. Li, I. Yang et al. 2010. "Drawing" upconversion nanophosphors into water through host-guest interaction. *Chem. Commun.* 46 (30):5551–5553.

Liu, X., M. Zheng, X. Kong et al. 2013. Separately doped upconversion-C_{60} nanoplatform for NIR imaging-guided photodynamic therapy of cancer cells. *Chem. Commun.* 49 (31):3224–3226.

Liu, Y., D. Tu, H. Zhu et al. 2013. Lanthanide-doped luminescent nanoprobes: Controlled synthesis, optical spectroscopy, and bioapplications. *Chem. Soc. Rev.* 42 (16):6924–6958.

Lucky, S. S., N. Muhammad Idris, Z. Li et al. 2015. Titania coated upconversion nanoparticles for near-infrared light triggered photodynamic therapy. *ACS Nano* 9 (1):191–205.

Luo, M., Q. Li, M. Chen et al. 2013. Controlled assembly of gold and rare-earth upconversion nanoparticles for ratiometric sensing applications. *Wuhan Univ. J. Nat. Sci.* 18 (4):277–282.

Ma, J., P. Huang, M. He et al. 2012. Folic acid-conjugated LaF_3:Yb,Tm@SiO_2 nanoprobes for targeting dual-modality imaging of upconversion luminescence and X-ray computed tomography. *J. Phys. Chem.* B 116 (48):14062–14070.

Ma, X. and X. Ni. 2015. Fabrication of polythiophene-TiO2 heterojunction solar cells coupled with upconversion nanoparticles. *J. Mater. Sci.: Mater. Electron.* 26 (2):1129–1135.

Mai, H.-X., Y.-W. Zhang, R. Si et al. 2006. High-quality sodium rare-earth fluoride nanocrystals: Controlled synthesis and optical properties. *J. Am. Chem. Soc.* 128 (19):6426–6436.

Muhr, V., S. Wilhelm, T. Hirsch et al. 2014. Upconversion nanoparticles: From hydrophobic to hydrophilic surfaces. *Acc. Chem. Res.* 47 (12):3481–3493.

Naccache, R., Yu Q., and Capobianco J. A. 2015. The fluoride host: Nucleation, growth, and upconversion of lanthanide-doped nanoparticles. *Adv. Opt. Mat.k.* 3 (4):482–509.

Niu, W., S. Wu, and S. Zhang. 2010. A facile and general approach for the multicolor tuning of lanthanide-ion doped $NaYF_4$ upconversion nanoparticles within a fixed composition. *J. Mater. Chem.* 20 (41):9113.

Oppenlander, T. 2003. *Photochemical Purification fo Water and Air.* Wiley-VCH Verlag GmbH & Co. KGaA, Weinheim.

Pan, L., M. He, J. Ma et al. 2013. Phase and size controllable synthesis of $NaYbF_4$ nanocrystals in oleic acid/ionic liquid two-phase system for targeted fluorescent imaging of gastric cancer. *Theranostics* 3 (3):210–222.

Park, Y. I., H. M. Kim, J. H. Kim et al. 2012. Theranostic probe based on lanthanide-doped nanoparticles for simultaneous in vivo dual-modal imaging and photodynamic therapy. *Adv. Mater.* 24 (42):5755–5761.

Park, Y. I., K. T. Lee, Y. D. Suh et al. 2015. Upconverting nanoparticles: A versatile platform for wide-field two-photon microscopy and multi-modal in vivo imaging. *Chem. Soc. Rev.* 44 (6):1302–1317.

Philipp, C. M., E. Rohde, and H. P. Berlien. 1995. Nd:YAG laser procedures in tumor treatment. *Semin. Surg. Oncol.* 11 (4):290–298.

Prodi, L., E. Rampazzo, F. Rastrelli et al. 2015. Imaging agents based on lanthanide doped nanoparticles. *Chem. Soc. Rev.* 44 (14):4922–4952.

Ramasamy, P., P. Manivasakan, and J. Kim 2014. Upconversion nanophosphors for solar cell applications. *RSC Adv.* 4 (66):34873–34895.

Ren, W., G. Tian, S. Jian et al. 2012. TWEEN coated $NaYF_4$:Yb,Er/$NaYF_4$ core/shell upconversion nanoparticles for bioimaging and drug delivery. *RSC Adv.* 2 (18):7037.

Ruggiero, E., J. Hernandez-Gil, J. C. Mareque-Rivas et al. 2015. Near infrared activation of an anticancer PtIV complex by Tm-doped upconversion nanoparticles. *Chem. Commun.* 51 (11):2091–2094.

Schäfer, H., P. Ptacek, K. Kömpe et al. 2007. Lanthanide-doped $NaYF_4$ nanocrystals in aqueous solution displaying strong up-conversion emission. *Chem. Mater.* 19 (6):1396–1400.

Sedlmeier, A. and H. H. Gorris. 2015. Surface modification and characterization of photon-upconverting nanoparticles for bioanalytical applications. *Chem. Soc. Rev.* 44 (6):1526–1560.

Shan, J. and Y. Ju. 2007. Controlled synthesis of lanthanide-doped $NaYF_4$ upconversion nanocrystals via ligand induced crystal phase transition and silica coating. *Appl. Phys. Lett.* 91 (12):123103.

Shan, J. and Y. Ju. 2009. A single-step synthesis and the kinetic mechanism for monodisperse and hexagonal-phase $NaYF_4$:Yb, Er upconversion nanophosphors. *Nanotechnology* 20:275603.

Shan, J., X. Qin, N. Yao et al. 2007. Synthesis of monodisperse hexagonal $NaYF_4$:Yb, Ln (Ln = Er, Ho and Tm) upconversion nanocrystals in TOPO. *Nanotechnology* 18 (44):445607.

Sun, L.-N., H. Peng, M. I. J. Stich et al. 2009. pH sensor based on upconverting luminescent lanthanide nanorods. *Chem. Commun.* (33):5000–5002.

Suyver, J. F., A. Aebischer, D. Biner et al. 2005. Novel materials doped with trivalent lanthanides and transition metal ions showing near-infrared to visible photon upconversion. *Opt. Mater.* 27 (6):1111–1130.

Tikhomirov, V. K., L. F. Chibotaru, D. Saurel et al. 2009. Er^{3+}-doped nanoparticles for optical detection of magnetic field. *Nano Lett.* 9 (2):721–724.

Topel, S. D., G. T. Cin, and E. U. Akkaya. 2014. Near IR excitation of heavy atom free Bodipy photosensitizers through the intermediacy of upconverting nanoparticles. *Chem. Commun.* 50 (64):8896–8899.

Tsang, M.-K., G. Bai, and J. Hao. 2015a. Stimuli responsive upconversion luminescence nanomaterials and films for various applications. *Chem. Soc. Rev.* 44 (6):1585–1607.

Tsang, M.-K., C.-F. Chan, K.-L. Wong et al. 2015b. Comparative studies of upconversion luminescence characteristics and cell bioimaging based on one-step synthesized upconversion nanoparticles capped with different functional groups. *J. Lumin.* 157:172–178.

Tu, L., X. Liu, F. Wu et al. 2015. Excitation energy migration dynamics in upconversion nanomaterials. *Chem. Soc. Rev.* 44 (6):1331–1345.

Valiente, R., M. Millot, F. Rodríguez et al. 2009. Er^{3+} luminescence as a sensor of high pressure and strong external magnetic fields. *High Pressure Res.* 29 (4):748–753.

Vetrone, F., R. Naccache, A. Juarranz De La Fuente et al. 2010a. Intracellular imaging of HeLa cells by non-functionalized $NaYF_4$:Er^{3+}, Yb^{3+} upconverting nanoparticles. *Nanoscale* 2 (4):495–498.

Vetrone, F., R. Naccache, A. Zamarrón et al. 2010b. Temperature sensing using fluorescent nanothermometers. *ACS Nano* 4 (6):3254–3258.

Viger, M. L., M. Grossman, N. Fomina et al. 2013. Low power upconverted near-IR light for efficient polymeric nanoparticle degradation and cargo release. *Adv. Mater.* 25 (27):3733–3738.

Voliani, V., M. Gemmi, L. Francés-Soriano et al. 2014. Texture and phase recognition analysis of β-$NaYF_4$ nanocrystals. *J. Phys. Chem. C* 118 (21):11404–11408.

Voliani, V., M. González-Béjar, V. Herranz-Pérez et al. 2013. Orthogonal functionalisation of upconverting $NaYF_4$ nanocrystals. *Chem. Eur. J.* 19 (40):13538–13546.

Wang, C., L. Cheng, Y. Liu et al. 2013. Imaging-guided pH-sensitive photodynamic therapy using charge reversible upconversion nanoparticles under near-infrared light. *Adv. Funct. Mater.* 23 (24):3077–3086.

Wang, C., H. Tao, L. Cheng et al. 2011. Near-infrared light induced in vivo photodynamic therapy of cancer based on upconversion nanoparticles. *Biomaterials* 32 (26):6145–6154.

Wang, D., B. Xue, X. Kong et al. 2015. 808 nm driven Nd^{3+}-sensitized upconversion nanostructures for photodynamic therapy and simultaneous fluorescence imaging. *Nanoscale* 7 (1):190–197.

Wang, F. and X. Liu 2009. Recent advances in the chemistry of lanthanide-doped upconversion nanocrystals. *Chem. Soc. Rev.* 38 (4):976–989.

Wang, G., Q. Peng, and Y. Li 2011. Lanthanide-doped nanocrystals: Synthesis, optical-magnetic properties, and applications. *Acc. Chem. Res.* 44 (5):322–332.

Wang, L., R. Yan, Z. Huo et al. 2005. Fluorescence resonant energy transfer biosensor based on upconversion-luminescent nanoparticles. *Angew. Chem. Int. Ed.* 44 (37):6054–6057.

Wang, M., G. Abbineni, A. Clevenger et al. 2011. Upconversion nanoparticles: synthesis, surface modification and biological applications. *Nanomedicine* 7 (6):710–729.

Wang, M., Z. Chen, W. Zheng et al. 2014. Lanthanide-doped upconversion nanoparticles electrostatically coupled with photosensitizers for near-infrared-triggered photodynamic therapy. *Nanoscale* 6 (14):8274–8282.

Wang, X., C. X. Yang, J. T. Chen et al. 2014. A dual-targeting upconversion nanoplatform for two-color fluorescence imaging-guided photodynamic therapy. *Anal. Chem.* 86 (7):3263–3267.

Wang, Y., H. Wang, D. Liu et al. 2013. Graphene oxide covalently grafted upconversion nanoparticles for combined NIR mediated imaging and photothermal/photodynamic cancer therapy. *Biomaterials* 34 (31):7715–7724.

Wei, Y., F. Lu, X. Zhang et al. 2006. Synthesis of oil-dispersible hexagonal-phase and hexagonal-shaped $NaYF_4$:Yb,Er nanoplates. *Chem. Mater.* 18 (24):5733–5737.

Wencel, D., T. Abel, and C. Mcdonagh. 2014. Optical chemical pH sensors. *Anal. Chem.* 86 (1):15–29.

Wilhelm, S., M. Kaiser, C. Wurth et al. 2015. Water dispersible upconverting nanoparticles: effects of surface modification on their luminescence and colloidal stability. *Nanoscale* 7 (4):1403–1410.

Wisser, M. D., M. Chea, Y. Lin et al. 2015. Strain-induced modification of optical selection rules in lanthanide-based upconverting nanoparticles. *Nano Lett.* 15 (3):1891–1897.

Wolfbeis, O. S. 2015. An overview of nanoparticles commonly used in fluorescent bioimaging. *Chem. Soc. Rev.* 44 (14):4743–4768.

Won Jin, K., N. Marcin, and N. P. Paras. 2009. Color-coded multilayer photopatterned microstructures using lanthanide (III) ion co-doped $NaYF_4$ nanoparticles with upconversion luminescence for possible applications in security. *Nanotechnology* 20 (18):185301.

Wu, S. and H.-J. Butt. 2015. Near-infrared-sensitive materials based on upconverting nanoparticles. *Adv. Mater.* doi: 10.1002/adma.201502843.

Wu, S., N. Duan, Z. Shi et al. 2014. Simultaneous aptasensor for multiplex pathogenic bacteria detection based on multicolor upconversion nanoparticles labels. *Anal. Chem.* 86 (6):3100–3107.

Wu, X., G. Chen, J. Shen et al. 2015. Upconversion nanoparticles: A versatile solution to multiscale biological imaging. *Bioconjug. Chem.* 26 (2):166–175.

Xia, L., X. Kong, X. Liu et al. 2014. An upconversion nanoparticle-Zinc phthalocyanine based nanophotosensitizer for photodynamic therapy. *Biomaterials* 35 (13):4146–4156.

Xiao, Q., Y. Ji, Z. Xiao et al. 2013. Novel multifunctional $NaYF_4$:Er^{3+},Yb^{3+}/PEGDA hybrid microspheres: NIR-light-activated photopolymerization and drug delivery. *Chem. Commun.* 49:1527–1529.

Xie, D., H. Peng, S. Huang et al. 2013. Core–shell structure in doped inorganic nanoparticles: Approaches for optimizing luminescence properties. *J. Nanomater.* 2013: 1–10.

Xie, J., Lee S., and Chen X. 2010. Nanoparticle-based theranostic agents. *Adv. Drug Deliver. Rev.* 62 (11):1064–1079.

Xie, L., Y. Qin, and H.-Y. Chen. 2012. Polymeric optodes based on upconverting nanorods for fluorescent measurements of pH and metal ions in blood samples. *Anal. Chem.* 84 (4):1969–1974.

Xing, Q., N. Li, Y. Jiao et al. 2015. Near-infrared light-controlled drug release and cancer therapy with polymer-caged upconversion nanoparticles. *RSC Adv.* 5 (7):5269–5276.

Yan, L., Y.-N. Chang, W. Yin et al. 2014. Biocompatible and flexible graphene oxide/upconversion nanoparticle hybrid film for optical pH sensing. *Phys. Chem. Chem. Phys.* 16 (4):1576–1582.

Yan, L., Y.-N. Chang, L. Zhao et al. 2013. The use of polyethylenimine-modified graphene oxide as a nanocarrier for transferring hydrophobic nanocrystals into water to produce water-dispersible hybrids for use in drug delivery. *Carbon* 57:120–129.

Yang, D., P. A. Ma, Z. Hou et al. 2015. Current advances in lanthanide ion (Ln^{3+})-based upconversion nanomaterials for drug delivery. *Chem. Soc. Rev.* 44 (6):1416–1448.

Yang, J., D. Shen, X. Li et al. 2012. One-step hydrothermal synthesis of carboxyl-functionalized upconversion phosphors for bioapplications. *Chemistry* 18 (43):13642–13650.

Yang, Y., B. Velmurugan, X. Liu et al. 2013. NIR photoresponsive crosslinked upconverting nanocarriers toward selective intracellular drug release. *Small* 9 (17):2937–2944.

Ye, X., J. E. Collins, Y. Kang et al. 2010. Morphologically controlled synthesis of colloidal upconversion nanophosphors and their shape-directed self-assembly. *PNAS* 107 (52):22430–22435.

Yi, G.-S. and G.-M. Chow. 2007. Water-soluble $NaYF_4$:Yb,Er(Tm)/$NaYF_4$/polymer core/shell/shell nanoparticles with significant enhancement of upconversion fluorescence. *Chem. Mater.* 19 (3):341–343.

Yi, G. S. and G. M. Chow. 2006. Synthesis of hexagonal-phase $NaYF_4$:Yb,Er and $NaYF_4$:Yb,Tm nanocrystals with efficient up-conversion fluorescence. *Adv. Funct. Mater.* 16 (18):2324–2329.

Yu, M., F. Li, Z. Chen et al. 2009. Laser scanning up-conversion luminescence microscopy for imaging cells labeled with rare-earth nanophosphors. *Anal. Chem.* 81 (3):930–935.

Zhang, S.-Z., L.-D. Sun, H. Tian et al. 2009. Reversible luminescence switching of $NaYF_4$:Yb,Er nanoparticles with controlled assembly of gold nanoparticles. *Chem. Commun.* (18):2547–2549.

Zhang, P., S. Rogelj, K. Nguyen et al. 2006. Design of a highly sensitive and specific nucleotide sensor based on photon upconverting particles. *J. Am. Chem. Soc.* 128 (38):12410–12411.

Zhang, Y.-W., X. Sun, R. Si et al. 2005. Single-crystalline and monodisperse LaF_3 triangular nanoplates from a single-source precursor. *J. Am. Chem. Soc.* 127 (10):3260–3261.

Zhou, A., Y. Wei, B. Wu et al. 2012. Pyropheophorbide a and c (RGDyK) comodified chitosan-wrapped upconversion nanoparticle for targeted near-infrared photodynamic therapy. *Mol. Pharmaceutics* 9:1580–1589.

Zhou, J., Q. Liu, W. Feng et al. 2015. Upconversion luminescent materials: Advances and applications. *Chem. Rev.* 115 (1):395–465.

Zhou, J., Y. Sun, X. Du et al. 2010. Dual-modality in vivo imaging using rare-earth nanocrystals with near-infrared to near-infrared (NIR-to-NIR) upconversion luminescence and magnetic resonance properties. *Biomaterials* 31 (12):3287–3295.

Zhou, L., Z. Chen, K. Dong et al. 2014. DNA-mediated construction of hollow upconversion nanoparticles for protein harvesting and near-infrared light triggered release. *Adv. Mater.* 26 (15):2424–2430.

Zhuravleva, N. G., A. A. Eliseev, N. A. Sapoletova et al. 2005. The synthesis of EuF_3/TOPO nanoparticles. *Mater. Sci. Eng.* C 25 (5–8):549–552.